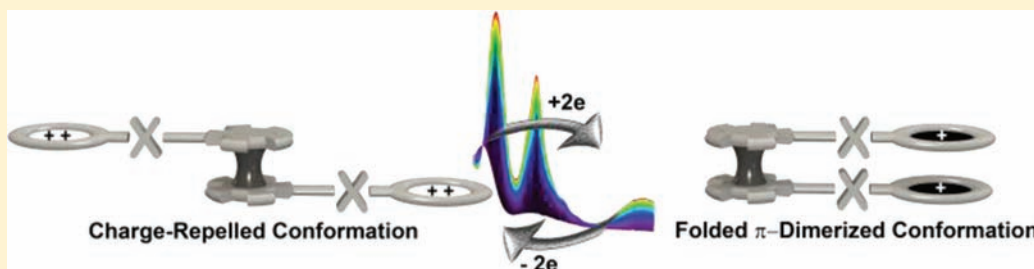


# Redox Control of Rotary Motions in Ferrocene-Based Elemental Ball Bearings

Adriana Iordache,<sup>†</sup> Mircea Oltean,<sup>‡</sup> Anne Milet,<sup>‡</sup> Fabrice Thomas,<sup>†</sup> Benoît Baptiste,<sup>§</sup> Eric Saint-Aman,<sup>†</sup> and Christophe Bucher<sup>\*†</sup>

<sup>†</sup>Laboratoire de Chimie Inorganique Rédox, <sup>‡</sup>Laboratoire de Chimie Théorique, and <sup>§</sup>Service de Crystallographie, Département de Chimie Moléculaire, Université Joseph Fourier/CNRS, Grenoble, France

**S** Supporting Information



**ABSTRACT:** Rotational motions of ferrocene-based carousels have been achieved by electron transfer centered on  $\pi$ -dimerizable 4,4'-bipyridinium substituents introduced on both cyclopentadienyl rings through covalent linkers of different size, geometry, and flexibility. Detailed spectroscopic, electrochemical, and theoretical analyses demonstrate that rigid and fully conjugated linkers allow the quantitative formation of intramolecular  $\pi$ -dimers resulting from optimized orbital overlaps within the HOMO of the electrochemically generated bis-radical species. The tetra-cationic “charge-repelled” conformers, the self-assembled  $\pi$ -dimers, and their electron triggered interconversions have been investigated by UV–vis, NMR, and ESR spectroscopy, electrochemistry, X-ray diffraction analysis, and theoretical calculations. These studies support the conclusion that the rotation of both cyclopentadienyl rings in ferrocene can be controlled electrochemically using noncovalent reversible interactions arising from  $\pi$ -radical coupling processes.

## INTRODUCTION

The ability to reversibly trigger fast movements of large amplitude in molecular objects has emerged in the past decade as a major scientific objective which is mainly motivated by exciting foreseen applications in nanosciences. From this promising and highly competitive field has already emerged a wide range of nanometer-scale analogues of macroscopic tools known as molecular gears, tweezers, switches, rotors, shuttles, brakes, and turnstiles, whose function is activated by light, temperature, or pH or through a wide range of chemical reactions.<sup>1</sup> Radical cation  $\pi$ -interactions have, for instance, been employed to generate mechanical motions in the form of translation as well as circumrotation in the context of mechanically interlocked molecules.<sup>2–4</sup>

Rotational motion is one of the most common and most important mechanical processes involved in energy conversion at different levels: from ATP synthases in mammalian cells, relying on ion fluxes and rotary motions of large proteins, to a range of macroscopic motors of fundamental importance for mankind. The control of rotational motion about molecular bonds is thus a primary but particularly challenging objective which has been intensively pursued using artificial inorganic or organic architectures.<sup>5</sup> Depending on the targeted applications, different types of rotary motions may be desirable. It might

serve as molecular switch, if one can reversibly flip a rotator into different readable positions using an external impulse, or as a machinery part, if the system is able to turn repeatedly and periodically in the same direction.<sup>6–12</sup>

Unsubstituted metallocenes, featuring two freely rotating cyclopentadienyl ligands (Cp) linked to a metal center,<sup>13,14</sup> have quite often been considered as archetypes of gear-wheels, propellers, or molecular carousels.<sup>15–19</sup> Wang or Crowley and co-workers have, for instance, recently devised various ferrocene-based rotors wherein intramolecular rotation is promoted chemically, by successive protonation/deprotonation of carboxylate or heteroaromatic fragments.<sup>16,17</sup> Photochemically controlled rotational motion of cyclopentadienyl ligands in ferrocene-based carousels has, on the other hand, only seldom been achieved, and most photo-operated systems have been developed by Aida and co-workers using an azobenzene strap.<sup>20–24</sup>

In the present article we describe the first example of a ferrocene-based redox-responsive molecular carousel whose rotating motion can be triggered by simple electron transfer centered on  $\pi$ -dimerizable bipyridinium groups introduced on the cyclopentadienyl rings of a ferrocene skeleton.

Received: October 17, 2011

Published: December 12, 2011

Scheme 1. Reversible Conversion of a Generic Ferrocene-Based Pivot between an "Open" Charge-Repelled Form and a "Closed"  $\pi$ -Dimerized State<sup>a</sup>

<sup>a</sup>X represents an organic linker.

The formation of  $\pi$ -bonded dimers from the spontaneous and reversible association of  $\pi$ -radicals has been observed with a wide range of polyaromatics, such as porphyrins, tetrafulvalenes, oligothiophenes, or viologenes.<sup>25–31</sup> Such noncovalent associations of  $\pi$ -radicals are characterized (i) by cofacial arrangements of monomeric moieties at interplanar distances of around  $3.05 \pm 0.25$  Å, matching the Cp–Cp distance found in ferrocene,<sup>26,32,33</sup> (ii) by diagnostic electronic absorption bands in the near-IR region, (iii) by silent ESR signatures, and (iv) by fast kinetics of dimerization. Observation of  $\pi$ -dimers usually requires nonstandard experimental conditions (low temperatures or high concentrations of radicals), but their formation is usually greatly favored in confined environments<sup>34</sup> or using structurally preorganized architectures<sup>35</sup> such as the propyl-linked bis-viologens allowing optimal overlap of two sets of singly occupied  $\pi$  orbitals from two adjacent reduced pyridinium rings.<sup>36–44</sup>

Our main motivation to carry out this work was to demonstrate that the redox properties of  $\pi$ -dimerizable bipyridiniums can be exploited to develop electron-motive rotating modules which could prove useful as molecular switches in electronics or as drivers for artificial molecular motors. The concept developed in this article is illustrated in Scheme 1. It involves the reversible conversion of a ferrocene pivot between an "open" charge-repelled form and a "closed" state wherein two reduced  $\pi$ -radicals adopt a cofacial arrangement promoting an efficient orbital overlap in a sandwich-like  $\pi$ -dimer.

## RESULTS AND DISCUSSION

**Synthesis.** Viologen moieties can potentially be appended to cyclopentadienyl (Cp) rings through a wide range of organic linkers. Several examples of ferrocene derivatives connected, through alkyl chains, to one 4,4'-bipyridinium moiety can be found in the literature,<sup>45–50</sup> but strategies allowing the introduction of one viologen per Cp fragment have been much less investigated.<sup>48,49,51</sup>

The road toward meeting our objectives required selecting linkers with suitable length, rigidity, and geometry to allow an optimal orbital overlap in the "closed" sandwich-like species (Scheme 1). In a first approach, we considered alkyl chains as flexible linkers between the metallocene and the electron deficient viologen (X in Scheme 1).

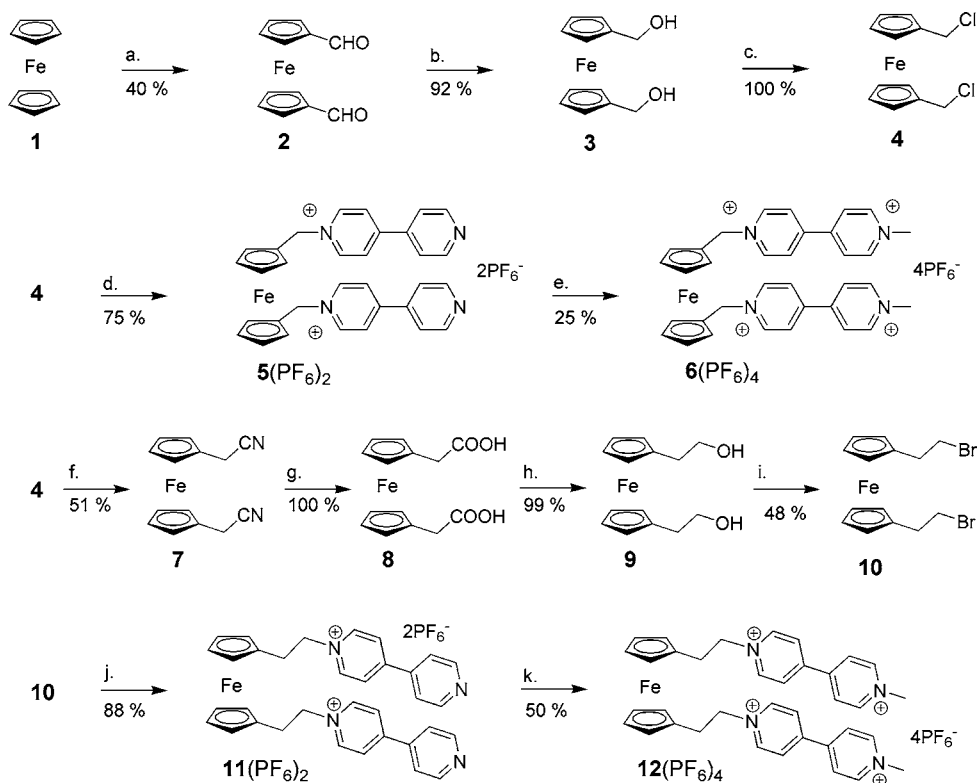
The synthesis of **6**(PF<sub>6</sub>)<sub>4</sub>, featuring a simple methylenic bridge between both bipyridiniums and the metallocene core,

has been achieved starting from ferrocene in an overall 7% yield, following a published procedure involving the 1,1'-di(chloromethyl)ferrocene **4** (Scheme 2) as a key intermediate.<sup>48,51</sup>

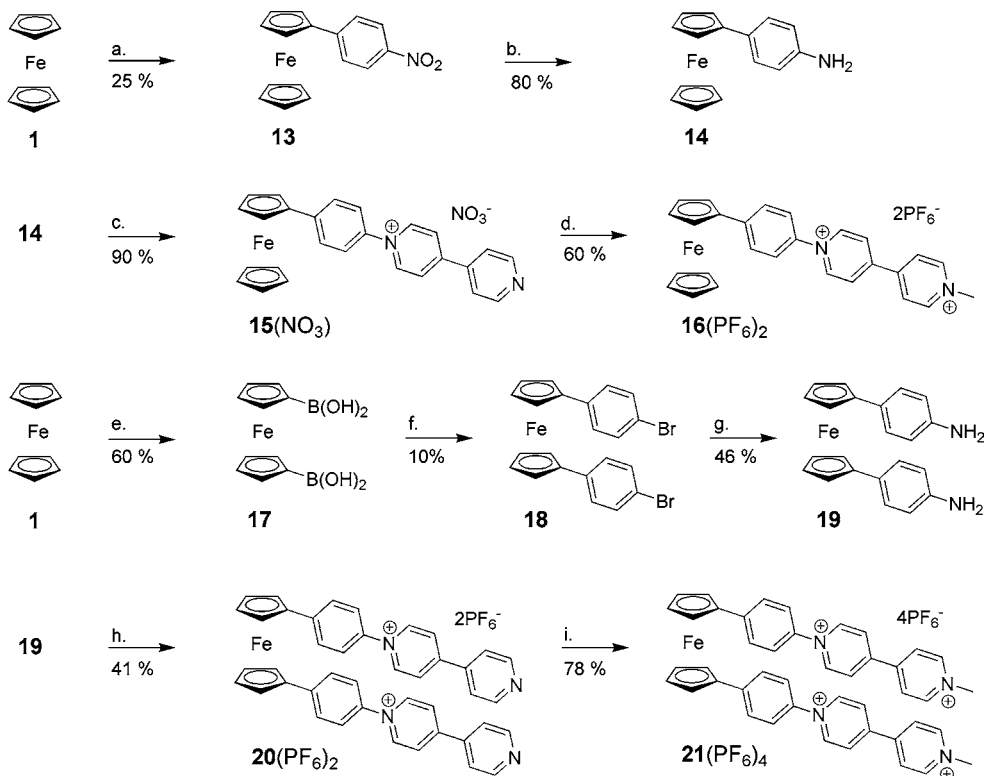
The introduction of a longer alkyl chain could be achieved through a classical homologation strategy starting from the chloromethylated derivative **4**. The latter could be converted in five steps with an overall 25% yield into the 1,1'-di(2-bromoethyl)ferrocene **10** via hydrolyzation of the 1,1'-di(cyanomethyl)ferrocene **7**<sup>52,53</sup> followed by reduction with LiAlH<sub>4</sub>, mesylation of the resulting bis-alcohol **9**,<sup>54</sup> and subsequent bromination in dry methylene chloride using lithium bromide (Scheme 2). It needs to be mentioned that the bis-brominated derivative **10** has previously been isolated through a nucleophilic cyclopropane ring-opening in spiro[2.4]hepta-4,6-diene with sodium [dicarbonyl( $\eta^5$ -cyclopentadienyl)ferrate] whereas longer homologues could be obtained by reduction of alkyl-carbonyl substituted ferrocenes.<sup>55–57</sup> In our hands, the direct formation of **10** from **9** could not be achieved using a classical brominating agent such as PBr<sub>3</sub><sup>58,59</sup> but only through the *in situ* formation of a mesylated intermediate ultimately converted into the bis-halogenated precursor **10**. Reacting this intermediate with an excess of 4,4'-bipyridine in acetonitrile produced the pyridine-pyridinium derivative **11**(PF<sub>6</sub>)<sub>2</sub>, readily isolated by simple filtration and further quaternized using methyl iodide. The targeted product **12**<sup>4+</sup> was finally isolated as a PF<sub>6</sub><sup>-</sup> salt through anion metathesis by addition of aqueous KPF<sub>6</sub> to the crude iodide precursor dissolved in water.

In a second approach, we aimed for derivatives wherein viologens and cyclopentadienyl rings are held at short distances through rigid connectors. As shown in Scheme 3, a benzene linkage could be introduced using aniline substituted ferrocenes as key intermediates. This ingenious strategy was mainly developed by Allen in the seventies<sup>60–64</sup> to cope with the poor reactivity of aryl halides prohibiting the direct formation of aryl-substituted pyridiniums.<sup>65</sup>

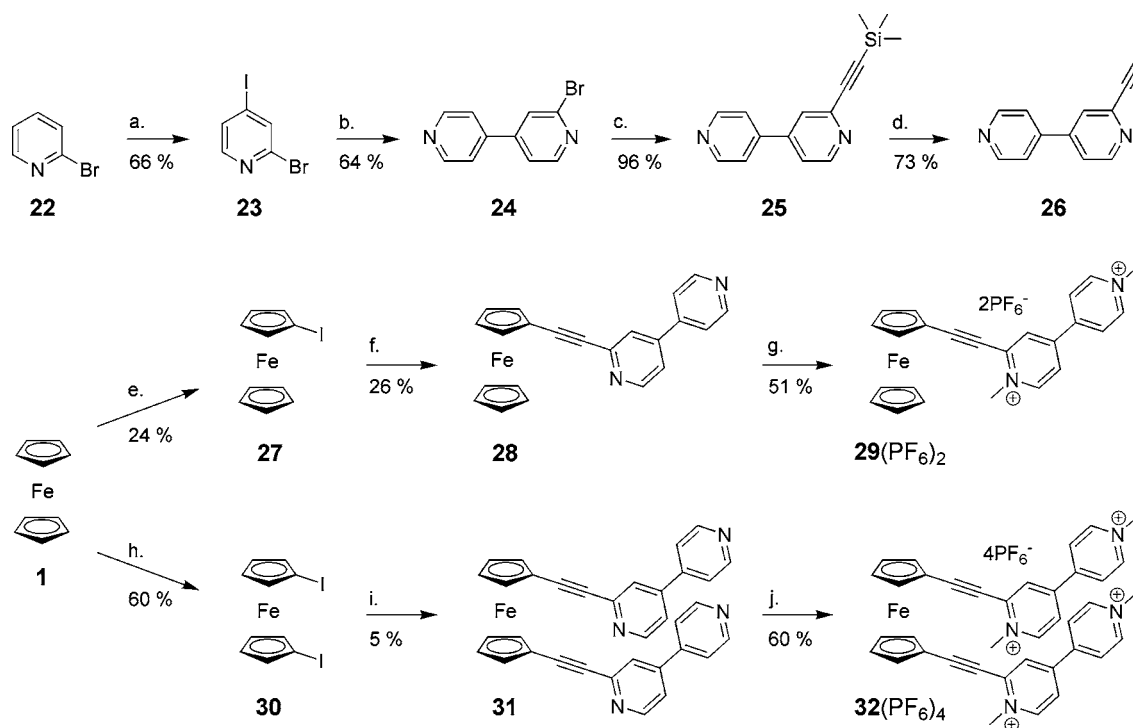
The monosubstituted 4-aminophenylferrocene **14** (Scheme 3) could be obtained following previously reported procedures<sup>66–69</sup> involving the diazotization of *p*-nitroaniline to form **13**, which was thereafter reduced in a Sn/HCl mixture. The relative efficiency and expediency of this procedure led us to hypothesize that a similar approach could be developed to produce the 1,1'-bis(4-aminophenyl)ferrocene derivative **19**, bearing an aniline side group on each Cp. Increasing the ratio

Scheme 2. Formation of the 1,1'-Di(2-Bromoethyl)ferrocene 10<sup>a</sup>

<sup>a</sup>Conditions: (a) *n*-BuLi/TMEDA/DMF; (b) NaBH<sub>4</sub>/MeOH; (c) PCl<sub>3</sub>/CH<sub>2</sub>Cl<sub>2</sub>; (d) 4,4'-bipyridine/CH<sub>3</sub>CN, KPF<sub>6</sub> aq; (e) CH<sub>3</sub>I/CH<sub>3</sub>CN, KPF<sub>6</sub> aq; (f) KCN aq; (g) KOH/EtOH; (h) LiAlH<sub>4</sub>/THF; (i) MsCl/Et<sub>3</sub>N then LiBr/CH<sub>2</sub>Cl<sub>2</sub>; (j) 4,4'-bipyridine/CH<sub>3</sub>CN, KPF<sub>6</sub> aq; (k) CH<sub>3</sub>I/CH<sub>3</sub>CN, KPF<sub>6</sub> aq.

Scheme 3. Introduction of a Benzene Linkage Using Aniline Substituted Ferrocenes as Key Intermediates<sup>a</sup>

<sup>a</sup>Conditions: (a) 4-Nitroaniline/NaNO<sub>2</sub>/HCl; (b) SnCl<sub>2</sub>/HCl/EtOH; (c) 1-(2,4-dinitrophenyl)-4,4'-bipyridinium chloride, CH<sub>3</sub>CN/EtOH abs; (d) CH<sub>3</sub>I/CH<sub>3</sub>CN/CH<sub>2</sub>Cl<sub>2</sub>; (e) *n*-BuLi/TMEDA/Et<sub>2</sub>O then B(OBu)<sub>3</sub>/Et<sub>2</sub>O; (f) 1-bromo-4-iodobenzene, Pd(dppf)Cl<sub>2</sub>, DME/NaOH 3 M; (g) Cu<sub>2</sub>O, DMF/NH<sub>3</sub> 28% water = 1/1; (h) 1-(2,4-dinitrophenyl)-4,4'-bipyridinium chloride, CH<sub>3</sub>CN/EtOH abs; (i) CH<sub>3</sub>I/CH<sub>3</sub>CN/CH<sub>2</sub>Cl<sub>2</sub>.

Scheme 4. Our Third Approach toward Rigidly Linked Viologen-Ferrocenes<sup>a</sup>

<sup>a</sup>Conditions: (a) LDA/THF/I<sub>2</sub> then LDA/THF; (b) pyridine-4-boronic acid, Pd(PPh<sub>3</sub>)<sub>4</sub>/NaHCO<sub>3</sub>/DME/H<sub>2</sub>O; (c) trimethyl silylacetylene, Pd(dppf)Cl<sub>2</sub>/THF/CuI/Et<sub>3</sub>N; (d) NaOH/MeOH; (e) *t*-BuLi/cyclohexane (nBu)<sub>3</sub>SnCl/THF then I<sub>2</sub>/CH<sub>2</sub>Cl<sub>2</sub>; (f) **26**, Pd(dppf)Cl<sub>2</sub>/CuI/THF/Et<sub>3</sub>N; (g) CH<sub>3</sub>I/CH<sub>3</sub>CN/CH<sub>2</sub>Cl<sub>2</sub>, KPF<sub>6</sub> aq; (h) *n*-BuLi/TMEDA/Et<sub>2</sub>O (nBu)<sub>3</sub>SnCl/THF then I<sub>2</sub>/CH<sub>2</sub>Cl<sub>2</sub>; (i) **26**, Pd(PPh<sub>3</sub>)<sub>4</sub>/THF/CuI/Et<sub>3</sub>N; (j) CH<sub>3</sub>I/CH<sub>3</sub>CN/CH<sub>2</sub>Cl<sub>2</sub>, KPF<sub>6</sub> aq Pd(dppf)Cl<sub>2</sub> = dichloro-((bis(diphenylphosphino))ferrocenyl) palladium(II).

of diazotized *p*-nitroaniline to ferrocene, however, turned out to systematically afford complex mixtures of polysubstituted ferrocenes isolated in low yields through fastidious purifications. This failure thus led us to develop a different approach, mainly inspired by the work of Braga and co-workers,<sup>70–72</sup> relying on the use of ferrocene-1,1'-diboronic acid, easily obtained from ferrocene and tributyl borate.<sup>73</sup> This boronic derivative (**17**) could be converted with a 5% yield into the targeted 1,1'-bis(4-aminophenyl)ferrocene **19** through the formation of the brominated intermediate **18**. The formation of aminoaryl derivatives from halogenated precursors is well documented,<sup>74</sup> but such a strategy has, to the best of our knowledge, never been implemented with ferrocene derivatives.

The aniline-appended ferrocenes **14** and **19** were ultimately converted in two steps into the targeted cationic species **16**(PF<sub>6</sub>)<sub>2</sub> and **21**(PF<sub>6</sub>)<sub>4</sub>, respectively. The initial step of these conversions requires the use of 1-(2,4-dinitrophenyl)-4,4'-bipyridinium chloride reacting with each aniline subunit to produce the targeted phenyl-substituted pyridine-pyridinium derivatives **15**(NO<sub>3</sub>) and **20**(PF<sub>6</sub>)<sub>2</sub>, wherein the positively charged nitrogen atom comes from the primary amine(s) in **14** or **19**.<sup>75</sup>

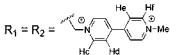
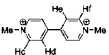
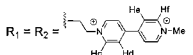
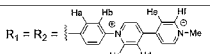
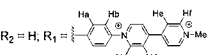
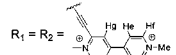
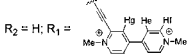
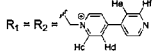
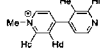
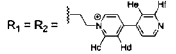
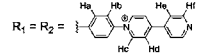
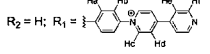
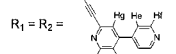
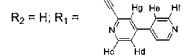
Our third approach toward rigidly linked viologen-ferrocenes is outlined in Scheme 4. The main objective was here to introduce an organic connector allowing minimization of the steric constraints between the metallocene and bipyridinium moieties.

The introduction of an ethynyl substituent on 4,4'-bipyridine could be achieved in four steps involving the bromination of one pyridine ring in the  $\alpha$ -position to a nitrogen atom. This novel brominated 4,4'-bipyridine (**24**) could be obtained in

64% yield through a Suzuki-like<sup>76</sup> palladium-catalyzed cross-coupling between the commercially available pyridine-4-boronic acid and the 2-bromo-4-iodopyridine **23**.<sup>77</sup> A Sonogashira coupling<sup>78</sup> between **24** and trimethyl silylacetylene subsequently afforded the intermediate **25**, which was readily deprotected to produce **26** in 73% yield. This viologen precursor was then coupled to the iodoferrocene **27**<sup>79</sup> under Sonogashira conditions to yield **28**, which was quaternized with methyl iodide in a mixture of CH<sub>3</sub>CN/CH<sub>2</sub>Cl<sub>2</sub> and ultimately submitted to an anion exchange procedure yielding the targeted compound **29**(PF<sub>6</sub>)<sub>2</sub>. A similar strategy developed from 1,1'-diiodoferrocene (**30**)<sup>80–82</sup> led to the rigidly linked bis-viologen ferrocene **32**(PF<sub>6</sub>)<sub>4</sub>.

**NMR Studies.** The targeted viologen-appended ferrocenes have been characterized by NMR spectroscopy using 1D and 2D NMR experiments. Signals attributed to the ferrocene fragment were observed between 4.0 and 4.2 ppm in the spectrum of **12**(PF<sub>6</sub>)<sub>4</sub>, between 4.2 and 4.6 ppm for **21**(PF<sub>6</sub>)<sub>4</sub>, and from 4.8 to 5.1 for the ethynyl bridged derivative **32**(PF<sub>6</sub>)<sub>4</sub>. The low-field shift experienced by these signals is unambiguously attributed to the electron withdrawing character of the bipyridinium fragments introduced on each Cp ligand. Such an effect is further brought to light through comparison of the latter values with the chemical shifts measured for Ha, Hb, and Hi in the monosubstituted derivatives **16**(PF<sub>6</sub>)<sub>2</sub> or **29**(PF<sub>6</sub>)<sub>2</sub> (Table 1). The number and the position of the <sup>1</sup>H NMR signals assigned to the hydrogen atoms of the pyridinium rings, observed between 7 and 9.3 ppm, are also significantly influenced by the nature and position of the organic linker, introduced either directly on the nitrogen atom, as in **6**(PF<sub>6</sub>)<sub>4</sub>,

Table 1.  $^1\text{H}$  NMR Chemical Shifts of Protons from the Heterocyclic Fragments in  $6^{4+}$ ,  $\text{DMV}^{2+}$ ,  $12^{4+}$ ,  $16^{2+}$ ,  $21^{4+}$ ,  $29^{2+}$ ,  $32^{4+}$ ,  $5^{2+}$ ,  $\text{MBP}^+$ ,  $11^{2+}$ ,  $15^+$ ,  $20^{2+}$ ,  $28$ , and  $31^{\text{a}}$ 

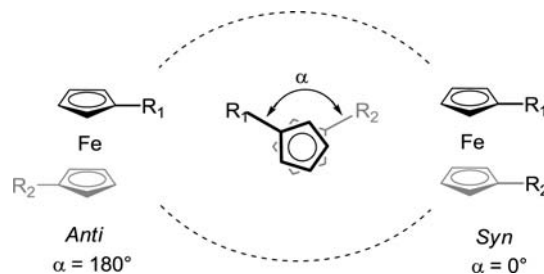
Compound	Ha	Hb	Hc	Hd	He	Hf	Hg
 $6(\text{PF}_6)_4$	-	-	8.83	8.33	8.33	8.98	-
 $\text{DMV}(\text{PF}_6)_2$	-	-	8.85	8.38	8.38	8.85	-
$\Delta\delta_1 = \delta(6^{4+}) - \delta(\text{DMV}^{2+})$	-	-	-0.02	-0.05	-0.05	0.13	-
 $12(\text{PF}_6)_4$	-	-	8.67	8.33	8.33	8.84	-
$\Delta\delta_2 = \delta(12^{4+}) - \delta(\text{DMV}^{2+})$	-	-	-0.18	-0.05	-0.05	-0.01	-
 $21(\text{PF}_6)_4$	7.77	7.70	8.90	8.48	8.59	9.20	-
 $16(\text{PF}_6)_2$	7.87	7.68	8.88	8.45	8.55	9.17	-
$\Delta\delta_3 = \delta(21^{4+}) - \delta(16^{2+})$	-0.1	0.02	0.02	0.03	0.04	0.03	-
 $32(\text{PF}_6)_4$	-	-	8.81	8.22	8.38	8.86	8.49
 $29(\text{PF}_6)_2$	-	-	8.76	8.16	8.38	8.85	8.43
$\Delta\delta_4 = \delta(32^{4+}) - \delta(29^{2+})$	-	-	0.05	0.06	0	0.01	0.06
 $5(\text{PF}_6)_2$	-	-	8.84	8.27	7.76	8.77	-
 $\text{MBP}(\text{PF}_6)$	-	-	8.85	8.29	7.78	8.71	-
$\Delta\delta_1 = \delta(5^{2+}) - \delta(\text{MBP}^+)$	-	-	-0.01	-0.02	-0.02	0.06	-
 $11(\text{PF}_6)_2$	-	-	8.84	8.23	7.76	8.53	-
$\Delta\delta_2 = \delta(11^{2+}) - \delta(\text{MBP}^+)$	-	-	-0.01	-0.07	-0.02	-0.18	-
 $20(\text{PF}_6)_2$	7.66	7.57	8.97	8.43	7.82	8.86	-
 $15(\text{PF}_6)$	7.84	7.65	9.03	8.48	7.88	8.89	-
$\Delta\delta_3 = \delta(20^{2+}) - \delta(15^+)$	-0.18	-0.08	-0.06	-0.05	-0.06	-0.03	-
 $31$	-	-	8.40	7.25	7.43	8.68	7.55
 $28$	-	-	8.67	7.48	7.63	8.76	7.73
$\Delta\delta_5 = \delta(31) - \delta(28)$	-	-	-0.27	-0.23	-0.20	-0.08	-0.18

<sup>a</sup>Recorded at 400 MHz in  $\text{CD}_3\text{CN}$  except for  $28$  and  $31$ , which have been recorded in  $\text{CD}_2\text{Cl}_2$ . Chemical shifts are reported in ppm using the solvent residual peak as internal standard. Differences between analogous mono- and disubstituted ferrocenes are denoted  $\Delta\delta_n$  ( $n = 1-5$ ).  $\text{DMV}^{2+}$  = dimethylviologen,  $\text{MBP}^+$  = 1-methyl-4,4'-bipyridinium.  $R_1$  and  $R_2$  are shown in Scheme 5.

$12(\text{PF}_6)_4$ , and  $21(\text{PF}_6)_4$ , or through one carbon atom of the pyridine ring in  $32(\text{PF}_6)_4$ .

Prior to this work, several NMR investigations have established that  $\pi-\pi$  interactions between aromatic substituents introduced on both Cp rings of a ferrocene might favor *syn*-like conformations (Scheme 5), with these intramolecular interactions being most of the time revealed through low field shifts in the aromatic region.<sup>16,83-87</sup>

The average resonance frequencies measured on the  $^1\text{H}$  NMR spectra of the bis-viologen derivatives  $6(\text{PF}_6)_4$ ,  $12(\text{PF}_6)_4$ ,  $21(\text{PF}_6)_4$ , or  $32(\text{PF}_6)_4$  result from the contribution of rotamers and conformers in equilibrium at a given temperature. Comparing these values with those corresponding to the monosubstituted compounds, used as references, thus came out

Scheme 5. Representation of Two Rotamers of Ferrocene: *anti* ( $\alpha = 180^\circ$ ) and *syn* ( $\alpha = 0^\circ$ )

as a straightforward way to assess the level of intramolecular interactions between both bipyridinium moieties. A large

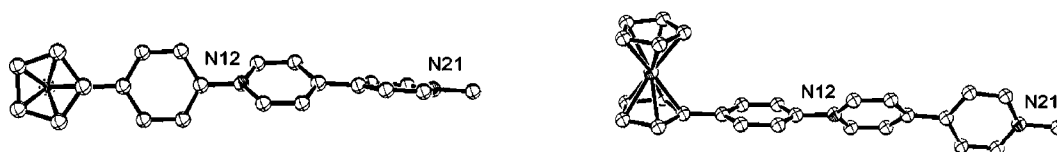


**Figure 1.** Top (left) and side (right) Ortep<sup>94</sup> views of **16**(PF<sub>6</sub>)<sub>2</sub>. Hydrogen atoms have been omitted for clarity reasons. Ellipsoids are drawn at a 45% probability level.

population of molecules in *syn*-conformation ( $\alpha \sim 0^\circ$  in Scheme 5), imposed by intramolecular stacking between the R<sub>1</sub> and R<sub>2</sub> side groups, would indeed lead to significant differences as opposed to *anti*-like conformations featuring non-interacting side groups.

The chemical shifts of signals attributed to the viologen side groups in the mono- and bis-substituted derivatives have been carefully analyzed, and the data are collected in Table 1. We find that the bipyridinium protons in the disubstituted alkyl-linked derivatives **6**<sup>4+</sup> and **12**<sup>4+</sup> resonate at frequency values matching those measured on the spectrum of 4,4'-dimethylbipyridinium (DMV<sup>2+</sup>) used as a reference. A similar conclusion can be drawn from comparison between **21**<sup>4+</sup> and **16**<sup>2+</sup> or between **32**<sup>4+</sup> and **29**<sup>2+</sup>. The picture which develops from this close examination is that the biscationic side groups introduced on each Cp's do not interact in acetonitrile, in agreement with simple electrostatic laws suggesting that positively charged units should repelled themselves and thus favor *anti*-like conformations. The mutual electrostatic repulsion of bipyridinium dicationic units is a well studied phenomenon which has been widely used, for instance by Stoddard's group to control mechanical motions in mechanically interlocked molecules.<sup>88–91</sup>

As recently established by Bosnich and co-workers, the conformation of polycationic 1,1'-diaryl ferrocenes is in fact driven by the balance of  $\pi$ -stacking “attracting” and electrostatic “repulsive” energies between positively charged aryl substituents introduced on the upper and lower rings of the metallocene framework.<sup>16</sup> To illustrate the utmost importance of electrostatic repulsion, mainly imposed by the number of positive charges borne by each substituents, the authors report that in solvents of high dielectric constant, such as CH<sub>3</sub>CN, the amount of torque generated by electrostatic repulsion in dicationic systems is insufficient to drive the two substituents away from populations where some  $\pi$ -overlap occurs. As an extension of this statement, our findings now demonstrate that the population of  $\pi$ -stacked states is negligible for tetra-cationic 1,1'-disubstituted ferrocenes, with the electrostatic repulsion being in the latter case much larger than the van der Waals attractive forces involved in  $\pi$  stacked assemblies. As expected from these conclusions, a different behavior is observed with the nonquaternized derivative **31**, showing aromatic <sup>1</sup>H NMR signals significantly shielded as compared to the same resonances in the monosubstituted derivative **28**. Shielding is strong for H<sub>c</sub> ( $\Delta\delta \sim 0.27$  ppm) and H<sub>d</sub> ( $\Delta\delta \sim 0.23$ ) and weak for H<sub>f</sub> ( $\Delta\delta \sim 0.08$ ), in agreement with a nonsymmetric conformation wherein the closest pyridine to the Cp ring experiences the greatest overlap. Such an arrangement is, however, not surprising, knowing that the interactions between dipolar or quadrupolar moments of aromatic fragments are known to favor offset-stacked geometries and disfavor perfectly stacked ones.<sup>92,93</sup>

This <sup>1</sup>H NMR study thus reveals that the tetra-cationic derivatives do not adopt *syn*-like arrangements in acetonitrile,

but it does not provide key information on their preferred conformations. Further insights into these conformational issues were obtained at the solid state by X-ray diffraction analyses and by computational chemistry.

**X-ray Diffraction Analyses.** Monocrystals of **16**(PF<sub>6</sub>)<sub>2</sub> have been grown in acetonitrile by slow diffusion of diisopropyl ether. The Ortep<sup>94</sup> views depicted in Figure 1 show both cyclopentadienes in an eclipsed conformation. The four covalently linked cyclic subunits (Cp-Ph-Py-Py) do not adopt a coplanar arrangement, as revealed by the large dihedral angles of 10.5°, 44.6°, and 30.4° measured between the Cp and benzene rings, between the benzene and the first pyridinium ring, and between both terminal pyridinium heterocycles, respectively.

Monocrystals of **11**(I)<sub>2</sub> have been grown by slow diffusion of tetra-*n*-butylammonium iodide into a solution of **11**(PF<sub>6</sub>)<sub>2</sub> in acetonitrile. Both Cp fragments adopt a slightly twisted conformation with an interplanar angle of around 2.3°. The angle measured between both bipyridinium axes (N8–N17) is 87.4°, and within each viologen, the pyridinium planes are found almost coplanar with a dihedral angle of only 5.5°. A careful examination of the crystal lattice furthermore reveals rather short intermolecular distances between two adjacent bipyridinium fragments ( $\sim 3.4$  Å). This proximity, as well as the coplanar conformation found within each viologen, indicates that the cationic charge is efficiently delocalized over all the bipyridinium units as compared to the case of the monoquaternized derivative shown in Figure 2. It also suggests that the conformation observed at the solid state is strongly influenced by supramolecular interactions.

Monocrystals of **12**(I)<sub>4</sub> have been grown by slow diffusion of tetra-*n*-butylammonium iodide into a solution of **12**(PF<sub>6</sub>)<sub>4</sub> in acetonitrile. The Ortep views depicted in Figure 3 reveal that the solid-state conformation of **12**(I)<sub>4</sub> is quite similar to that of its dicationic precursor **11**(I)<sub>2</sub>. The Cp ligands are found in an eclipsed geometry (interplanar Cp–Cp angle  $\sim 3.2^\circ$ ), and the angle measured between both bipyridinium substituents (N17–N8 and N108–N117) is 78.2° (Figure 3). As seen for **11**<sup>2+</sup>, the conformation observed at the solid state is mainly imposed by a wide range of intermolecular interactions involving the cyclopentadiene and bipyridium units acting as a donor and acceptor, respectively. The partial view of the crystal packing reveals, for instance, a cofacial arrangement of both subunits with intermolecular carbon–carbon distances as low as 3.25 Å (Figure 3). The conformation of each molecule and their organization in the crystal lattice is further imposed by a compact network of hydrogen bonds involving the pyridinium units, iodide anions, and solvent molecules (not shown in Figure 4).

Overall, these results are in agreement with the absence of intramolecular interactions between the bipyridium units, but they can hardly be utilized as definitive proofs, revealing what is the preferred conformation of the bis-viologen derivatives in solution. Crystal packing effects and intermolecular interactions

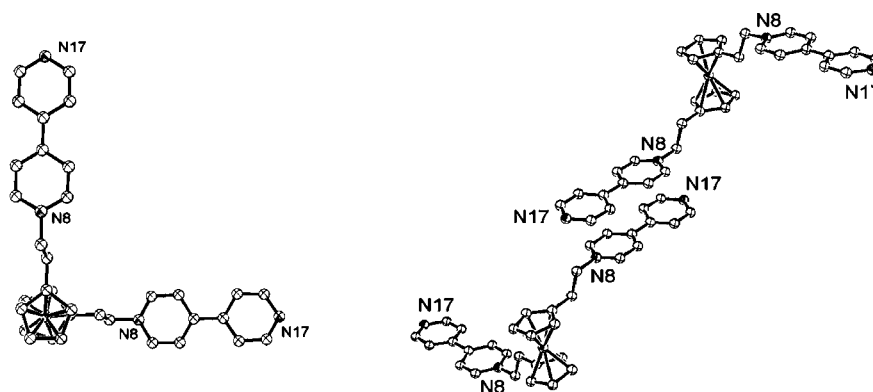


**Figure 2.** Ortep<sup>94</sup> views of **11(I)**<sub>2</sub>. Top (left) and partial (right) views of the crystal packing. Hydrogen atoms have been omitted for clarity reasons. Ellipsoids are drawn at a 50% probability level.

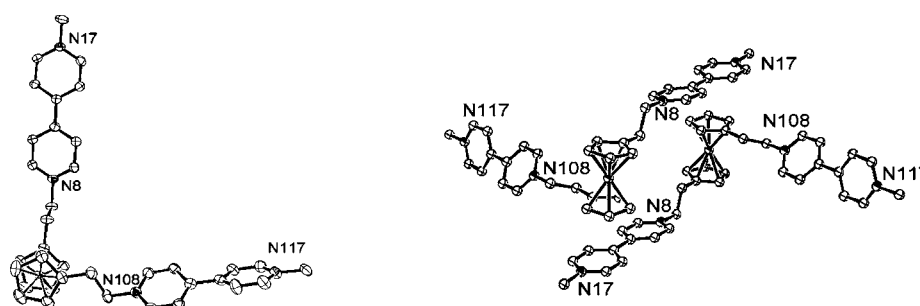


**Figure 3.** Ortep<sup>94</sup> views of **12(I)**<sub>4</sub>. Top (left) and partial (right) views of the crystal packing. Hydrogen atoms have been omitted for clarity reasons. Ellipsoids are drawn at a 50% probability level.

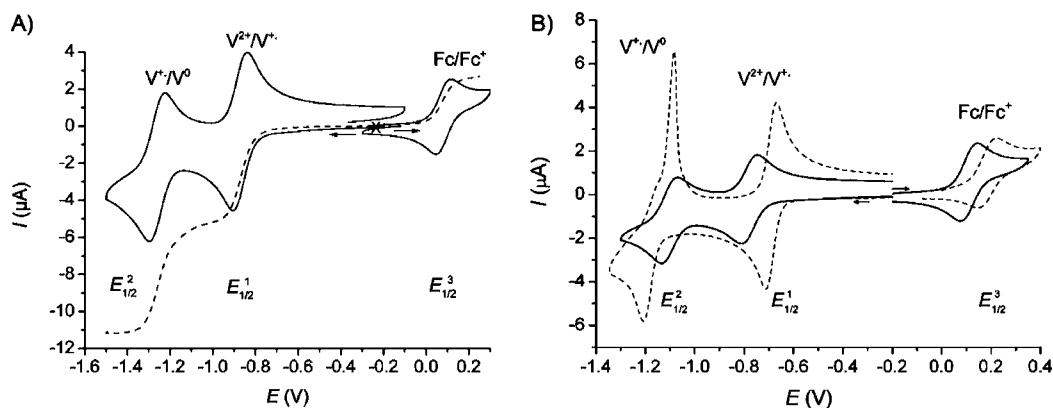


**Figure 4.** (A) Voltammetric curves of a DMF (TBAP 0.1 M) solution of **12(PF<sub>6</sub>)<sub>4</sub>** ( $5 \times 10^{-4}$  M) recorded at (solid line) a stationary platinum working electrode ( $\varnothing = 2$  mm,  $E$  vs  $\text{Ag}/\text{Ag}^+$  ( $10^{-2}$  M),  $\nu = 0.1$  V·s<sup>-1</sup>) and (dotted line) at a rotating platinum disk electrode ( $\varnothing = 2$  mm,  $\nu = 0.01$  V·s<sup>-1</sup>, 550 rd/min). (B) Voltammetric curves of DMF (TBAP 0.1 M) solutions of **16(PF<sub>6</sub>)<sub>2</sub>** (solid line) and **21(PF<sub>6</sub>)<sub>4</sub>** (dotted line) ( $5 \times 10^{-4}$  M) recorded at (solid line) a stationary platinum working electrode ( $\varnothing = 2$  mm,  $E$  vs  $\text{Ag}/\text{Ag}^+$  ( $10^{-2}$  M),  $\nu = 0.1$  V·s<sup>-1</sup>).

involved at the solid state are clearly too important to allow a meaningful comparison with data collected in liquid phases.

**Electrochemical Investigations.** The electrochemical activity of the mono- and disubstituted ferrocenes has been studied in DMF (0.1 M TBAP) using cyclic voltammetry (CV) and voltammetry at rotating disk electrodes (RDE). The CV curves exhibit similar patterns showing both well-known consecutive viologen-centered reversible reductions as well as, in the positive potential domain, the reversible one-electron oxidation of ferrocene (Figure 4). The number of electrons exchanged in each process is easily estimated through RDE measurements (dotted lines in Figure 4A), yielding three

diffusion waves whose relative intensities are directly proportional to the number of viologens and ferrocenes in the structure. The electrochemical data corresponding to each derivative are collected in Table 2.

It should be pointed out that the half-wave potential of ferrocene varies over a large domain from 0.08 V for **12<sup>4+</sup>** up to 0.57 V measured with **32<sup>4+</sup>**. We believe that these changes observed in the series result from a combination of “through bond” and “through space” electron withdrawing effects of the bipyridinium fragments on the ferrocene center. In **32<sup>4+</sup>**, the ethynyl linkers introduced between the Cp rings and the deficient bipyridinium units allow an efficient electron

Table 2. Half Wave Potential ( $E_{1/2}$ ) Measured by Cyclic Voltammetry<sup>a</sup>

	$E_{1/2}^1$ (V) $V^{2+}/V^{+•}$	$\Delta E_p^1$ (mV) $V^{2+}/V^{+•}$	$E_{1/2}^2$ (V) $V^{+•}/V^0$	$E_{1/2}^3$ (V) $Fc^{2+}/Fc^{3+}$	$\Delta E^0$ (mV) ( $V^{2+}/V^{+•}$ )	$K_{Disp}^d$ ( $\times 10^{-3}$ )	$K_{Dim}^e$
DMV(PF <sub>6</sub> ) <sub>2</sub>	-0.83(1)	64	-1.19(1)				
6(PF <sub>6</sub> ) <sub>4</sub>	-0.86(2)	70	-1.24(2)	0.34(1)	48	155	
12(PF <sub>6</sub> ) <sub>4</sub>	-0.86(2)	64	-1.25(2)	0.08(1)	42	196	
16(PF <sub>6</sub> ) <sub>2</sub>	-0.78(1)	62	-1.10(1)	0.11(1)			
21(PF <sub>6</sub> ) <sub>4</sub>	-0.69(2)	39	<i>b</i>	0.18(1)	-15	1818	1248
29(PF <sub>6</sub> ) <sub>2</sub>	-0.84(1)	64	-1.18(1)	0.32(1) <sup>c</sup>			
32(PF <sub>6</sub> ) <sub>4</sub>	-0.74(2)	46	-1.24(2)	0.57(1) <sup>c</sup>	13	613	2756

<sup>a</sup>Measured by CV,  $5 \times 10^{-4}$  M in DMF + TBAP (0.1 M), platinum working electrode  $\varnothing = 2$  mm,  $E$  vs Ag/Ag<sup>+</sup> ( $10^{-2}$  M), 298 K, CV:  $\nu = 0.1$  V·s<sup>-1</sup>; RDE:  $\nu = 0.01$  V·s<sup>-1</sup>, 550 rd/min;  $\Delta E_p^1$  measured at  $\nu = 0.02$  V·s<sup>-1</sup> using an automatic ohmic drop compensation procedure.  $\Delta E^0 = E_{1-1}^0 - E_{1-2}^0$  was estimated using a method established by Richardson *et al.*<sup>95</sup> The number of electrons transferred for each electrochemical process is shown between parentheses. <sup>b</sup>Adsorption phenomena lead to ill-behaved voltammograms. <sup>c</sup>Irreversible wave. <sup>d</sup> $K_{Disp}$  calculated from  $\log_{10}(K_{disp}) = -\Delta E^0/0.059$ .<sup>95,96</sup> <sup>e</sup> $K_{Dim}$  estimated from  $K_{dim} = \exp[(E_{1/2}^1 - (E_{1/2}^1)_{ref})/(RT/nF)]$  (see Supporting Information).

delocalization over the entire molecule; the shift of the ferrocene oxidation potential toward more positive values thus more likely results from this conjugation, which greatly amplifies the bipyridiniums' withdrawing effects and considerably lowers the electron density on the metallic center. This effect is not so important with the less conjugated phenyl-linked derivative **21**<sup>4+</sup> and almost negligible with **12**<sup>4+</sup>, featuring a saturated ethylene linker which limits the extent of the electronic communication between the bipyridinium and ferrocene centers. Following a similar reasoning, we believe that the large positive oxidation potential measured with **6**<sup>4+</sup> mainly results from "through space" electrostatic effects imposed by the structure of the methylene linker leading to relatively short distances between the dicationic bipyridiniums and the ferrocene centers.

We also find that the redox signature of *N,N'*-dimethyl-4,4'-bipyridinium (DMV<sup>2+</sup>), studied as a reference featuring two consecutive reversible one-electron reduction waves, exhibits strong similarities with that of the alkyl-linked ferrocene viologens **6**<sup>4+</sup> and **12**<sup>4+</sup>. The  $E_{1/2}^1$  and  $\Delta E_p^1$  values measured for these derivatives indeed suggest that the "communication" between the bipyridinium and ferrocene groups is negligible and that each redox-active subunit behaves as an independent center. The  $\Delta E_p^1$  values found between 70 and 64 mV for **6**<sup>4+</sup> and **12**<sup>4+</sup>, moreover, not only fall within the same range, they also do correspond to what is expected for molecules featuring two chemically equivalent and non-interacting redox-active centers. In other words, these electrochemical data can be seen as clear experimental evidence demonstrating that both bipyridium moieties are not interacting in solution, neither in their standard dicationic state nor after reduction, as cation radical species.<sup>96,97</sup>

A fully different conclusion is inferred from the signature of the "rigid" systems **21**<sup>4+</sup> and **32**<sup>4+</sup>, wherein ferrocene and bipyridinium moieties are connected through alkyne or phenyl linkers: (i) The first reduction process proceeds in both cases at significantly less negative potential values in the 1,1'-disubstituted ferrocenes than in the monosubstituted ones. The first viologen-centered reduction is observed at  $E_{1/2}^1 = -0.69$  and  $-0.74$  V for **21**(PF<sub>6</sub>)<sub>4</sub> and **32**(PF<sub>6</sub>)<sub>4</sub>, respectively, and at  $E_{1/2}^1 = -0.78$  and  $-0.84$  V for the corresponding monosubstituted analogues **16**(PF<sub>6</sub>)<sub>2</sub> and **29**(PF<sub>6</sub>)<sub>2</sub>, respectively (Figure 4B); (ii) The  $\Delta E_p^1$  values of 39 and 46 mV measured on the first reduction wave of **21**(PF<sub>6</sub>)<sub>4</sub> and **32**(PF<sub>6</sub>)<sub>4</sub>, respectively, are much smaller than those of 62 and 64 mV found under the same conditions with the corresponding references **16**(PF<sub>6</sub>)<sub>2</sub> and **29**(PF<sub>6</sub>)<sub>2</sub>. These

electrochemical data, in marked contrast with those reported above for the alkyl-linked ferrocene-viologens, can be explained considering a complex mechanism involving coupled electrochemical (E) and chemical (C) processes. The electrochemical behavior of molecules with multiple redox centers has already been thoroughly investigated.<sup>98,99</sup> It has been demonstrated that electron transfers to or from molecules containing identical, non-interacting, electroactive centers should yield a single current-potential CV curve similar to that observed with a single one electron electroactive center ( $\Delta E_p = 58$  mV at 25 °C) but with a magnitude determined by the total number of redox centers. When each center is characterized by the same standard potential  $E_m^0$  and adheres to the Nernst equation, it is possible to calculate the formal potentials corresponding to each pair of  $n$  successive oxidation states of the multicenter molecules. Considering fully non-interacting centers, the theoretical shift between the first viologen-based formal reduction potentials ( $E_{1-1}^0$  and  $E_{1-2}^0$  in Figure 5) should thus

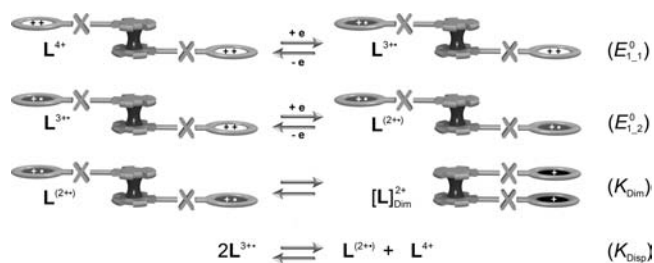


Figure 5. Successive one electron reductions of a generic 1,1'-bis(bipyridinium)ferrocene  $L^{4+}$  ( $E_{1-1}^0$  and  $E_{1-2}^0$ ) and their potential coupled chemical reactions: dimerization ( $K_{Dim}$ ) and disproportionation ( $K_{Disp}$ ).

equal  $\Delta E_1^0 = E_{1-2}^0 - E_{1-1}^0 = 35.6$  mV, although both redox processes are expected to appear as a single wave with peak potentials satisfying  $\Delta E_p = 58$  mV. Experimentally, the lowest  $\Delta E_p$  value has been recorded with **21**<sup>4+</sup> ( $\Delta E_p^1 = 39$  mV), in which two chemically equivalent bipyridiniums, linked through a ferrocene pivot, are successively reduced into **21**<sup>3+•</sup> and **21**<sup>2+••</sup> ( $E_{1-1}^0$  and  $E_{1-2}^0$  in Figure 5). Such a low  $\Delta E_p$  value thus reveals that the bipyridinium centers do not behave independently, as postulated in the theoretical description discussed above, and that they do interact as their reduced radical states to form the  $\pi$ -dimer complexes denoted  $[L]_{Dim}^{2+}$ .<sup>26,27</sup>

As mentioned in the introduction, these sandwich-like dimers are, most of the time, only observed at very low temperatures or at high concentrations of simple viologen radicals as well as



in confined environments or with structurally preorganized architectures.<sup>36–39,100,101</sup>

The low  $\Delta E_p$  value recorded with **21**<sup>4+</sup> and **32**<sup>4+</sup> thus unambiguously results from the intramolecular association between both bipyridinium radicals ( $K_{\text{dim}}$  in Figure 5), which shifts the second viologen-centered reduction ( $E_{1,2}^0$ ) at a less negative potential value than the initial one ( $E_{1,1}^0$ ). As shown in Figure 5, the exact mechanism involves two cathodic electron transfer processes and two coupled chemical steps: the intramolecular dimerization of two radicals producing a  $\pi$ -dimer ( $K_{\text{dim}}$ ) and a disproportionation equilibrium, with log  $K_{\text{disp}} = -\Delta E^0/0.059$ .<sup>95</sup>

In a first approximation,  $K_{\text{disp}}$ ,  $K_{\text{dim}}$ , as well as  $E_{1,2}^0$  and  $E_{1,1}^0$  have been calculated from the  $\Delta E_p$  and  $E_{1/2}$  values measured by cyclic voltammetry.<sup>95</sup> As shown in Table 2, the  $\Delta E^0$  and  $K_{\text{Disp}}$  values estimated for the bis(bipyridinium) derivatives are in agreement with our initial assumptions relying on simple comparisons between the  $E_{1/2}$  and  $\Delta E_p$  values. The lowest disproportionation constants are found with the alkyl linked derivatives **6**<sup>4+</sup> and **12**<sup>4+</sup>, behaving as an assembly of independent redox centers, whereas both rigid species exhibit much larger  $K_{\text{Disp}}$  values ( $613 \times 10^{-3} \text{ M}^{-1}$  and  $1818 \times 10^{-3} \text{ M}^{-1}$ ) due to more favorable intramolecular  $\pi$ -dimerizations ( $K_{\text{dim}}, \text{L}^{2(+\bullet)} \rightarrow [\text{L}]_{\text{Dim}}^{2+}$ ), resulting in the displacement of the disproportionation equilibrium toward the doubly reduced species  $\text{L}^{2(+\bullet)}$ .

It needs to be mentioned that the intramolecular dimerization following the first electron transfers additionally shifts the second reduction potential, leading to the neutral bipyridinium species.<sup>88,102</sup> The  $E_{1/2}^0$  value is, for instance, found at a significantly lower value in **32**<sup>4+</sup> than in the monomer **29**<sup>2+</sup>, as a consequence of the stabilizing influence of the radical-coupling involved in the  $\pi$ -dimerization process. A similar potential shift is observed between **16**<sup>2+</sup> and **21**<sup>4+</sup> (Figure 4B), although, in the later case, the ill-behaved shape of the second reduction wave ( $V^{+\bullet}/V^0$ ) suggests the existence of adsorption phenomena.

These electrochemical data thus support the notion that the geometric and structural features of the rigid systems **21**<sup>4+</sup> and **32**<sup>4+</sup> allow an efficient redox-triggered rotation of the ferrocene pivot driven by the formation of an intramolecular  $\pi$ -dimer.

**Spectro-electrochemical Investigations.** The UV–vis absorption data of the bipyridinium-appended ferrocenes are collected in Table 3. The alkyl-linked derivatives exhibit an

**Table 3. Absorption Wavelengths and Extinction Coefficients Associated with the Absorption Bands Observed in the Spectra of the Ferrocene-Viologen Derivatives<sup>a</sup>**

	$\lambda$ (nm); $\epsilon$ (L·mol <sup>-1</sup> ·cm <sup>-1</sup> )		
DMV(PF <sub>6</sub> ) <sub>2</sub>	264; 19500		
<b>6</b> (PF <sub>6</sub> ) <sub>4</sub>	265; 45300	472; 1000	
<b>12</b> (PF <sub>6</sub> ) <sub>4</sub>	266; 42000	477; 2300	
<b>16</b> (PF <sub>6</sub> ) <sub>2</sub>	275; 23300	357; 9500	546; 1800
<b>21</b> (PF <sub>6</sub> ) <sub>4</sub>	266; 49000	355; 21000	565; 1700
<b>29</b> (PF <sub>6</sub> ) <sub>2</sub>	267; 25000	368; 13300	567; 3200
<b>32</b> (PF <sub>6</sub> ) <sub>4</sub>	265; 48200	368; 24000	541; 6200

<sup>a</sup>All measurements have been performed in DMF electrolyte (0.1 M TBAP) at a concentration of 10<sup>-4</sup> M in viologen units.

intense viologen-centered  $\pi$ – $\pi^*$  transition<sup>103</sup> in the UV range, between 260 and 280 nm ( $42000 < \epsilon < 45000 \text{ L}\cdot\text{mol}^{-1}\cdot\text{cm}^{-1}$ ), and a less intense iron-based d–d transition around 460 nm

( $1000 < \epsilon < 2500 \text{ L}\cdot\text{mol}^{-1}\cdot\text{cm}^{-1}$ ).<sup>104</sup> The connection between a ferrocene donor and one or two organic electron-acceptors through conjugated linkers leads to large hyperchrome and bathochrome shifts in the visible range.<sup>105–107</sup> It also results in a significant photosensitivity going from moderate with the phenyl-substituted derivatives **16**<sup>2+</sup> and **21**<sup>4+</sup> to relatively important for the alkyne-linked systems **29**<sup>2+</sup> and **32**<sup>4+</sup>. As a consequence, these compounds were systematically handled and studied in the absence of light.

In-situ spectroelectrochemical analyses were carried out to obtain further insights into the nature of the electrogenerated species. For these investigations, absorption spectra were recorded periodically as the ferrocene-viologenes were submitted to bulk electrolyses. Electrochemical reductions of DMV<sup>2+</sup> (up to 1 electron/molecule), **6**<sup>4+</sup>, and **12**<sup>4+</sup> (up to 2 electrons/molecule), performed in anhydrous DMF electrolyte in the potentiostatic regime upon setting the potential of a platinum working electrode at –1 V, produced similar spectroscopic patterns with a large decrease in intensity of the initial  $\pi$ – $\pi^*$  absorption band at the expense of new signals growing at  $\lambda_{\text{max}} = 400 \text{ nm}$  ( $\epsilon = 80000 \text{ L}\cdot\text{mol}^{-1}\cdot\text{cm}^{-1}$ ) and at 610 nm ( $\epsilon = 30000 \text{ L}\cdot\text{mol}^{-1}\cdot\text{cm}^{-1}$ ) with shoulders from 530 to 800 nm (Figure 6). The blue color and UV–vis signature of the resulting solutions could thus be attributed to the non-associated bipyridinium cation radical DMV<sup>+•</sup><sup>75</sup> and bis-radicals **6**<sup>2(+•)</sup> and **12**<sup>2(+•)</sup>, respectively ( $\text{L}^{2(+\bullet)}$  in Figure 5). The reversibility of the reduction process at the electrolysis time scale was moreover checked by UV–vis absorption spectroscopy and voltammetry at rotating disk electrodes upon recovering the entire signature of the initial species after back electron transfer.

These assumptions were further confirmed upon analyzing samples of the electrolyzed solutions by ESR spectroscopy (Figure 7). The latter were collected after full electrochemical reduction of each viologen fragment in **6**(PF<sub>6</sub>)<sub>4</sub>, **12**(PF<sub>6</sub>)<sub>4</sub>, or DMV(PF<sub>6</sub>)<sub>2</sub>. The ESR spectra recorded at room temperature in DMF electrolyte show one signal at  $g = 2.00$  attributed to the  $S = 1/2$  organic radicals DMV<sup>+•</sup>, **6**<sup>2(+•)</sup>, and **12**<sup>2(+•)</sup> (Figure 8). It should, however, be noted that a hyperfine splitting<sup>108,109</sup> is observed only with DMV<sup>+•</sup>, whereas broad and unresolved signals were obtained with the less symmetric species **6**<sup>2(+•)</sup> and **12**<sup>2(+•)</sup>.

These results point out the incapacity of both bipyridinium radicals in **6**<sup>2(+•)</sup> and **12**<sup>2(+•)</sup> to self-assemble into  $\pi$ -dimer complexes, at least in DMF at room temperature. In an attempt to find experimental conditions which would favor the dimerization, we studied the effect of temperature or the influence of added water in the electrolyte.<sup>110</sup> Solutions of **6**<sup>2(+•)</sup>, **12**<sup>2(+•)</sup>, and DMV<sup>+•</sup> in THF/DMF (50/50 v/v), obtained by bulk electrolyses conducted at room temperature under an argon atmosphere, were slowly cooled down to 193 K. These drastic temperature changes turned out to have no influence on the reference compound DMV<sup>+•</sup> and on **6**<sup>2(+•)</sup> as opposed to **12**<sup>2(+•)</sup>, whose absorption spectrum was seen to gradually evolve upon cooling. As seen in Figure 8B, the intensity of the main signals centered initially at 400 and 610 nm on the spectrum of **12**<sup>2(+•)</sup> goes down as the temperature is lowered at the expense of new bands growing at lower wavelengths, 360 and 520 nm, respectively, and of a new broad signal in the near-infrared region (above 800 nm).

Similar results were obtained at room temperature using an aqueous electrolyte. Although these investigations were greatly hampered by the limited solubility of all the ferrocene-viologenes

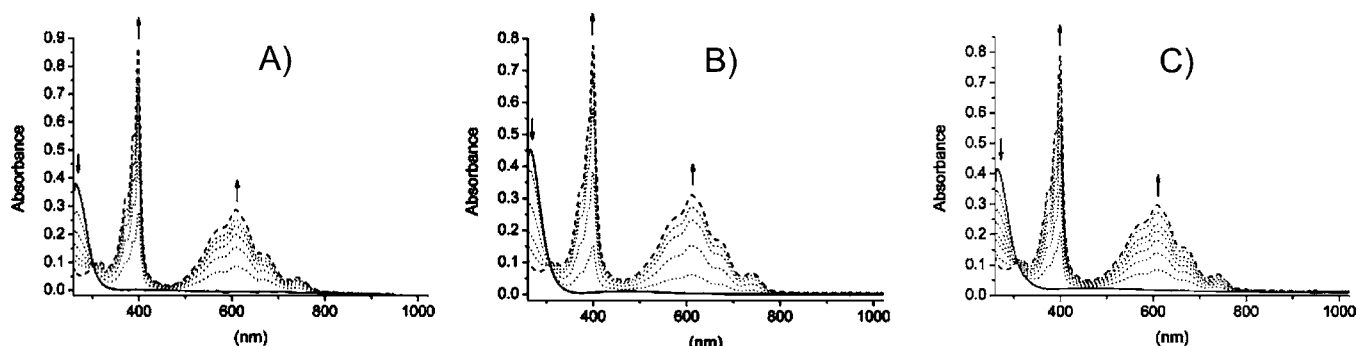


Figure 6. UV-vis spectra recorded during the exhaustive one-electron reduction (per viologen) of (A)  $6(\text{PF}_6)_4$ , (B)  $12(\text{PF}_6)_4$ , and (C)  $\text{DMV}(\text{PF}_6)_2$  in DMF (0.1 M TBAP) using a platinum plate working electrode ( $\sim 10 \text{ cm}^2$ ) whose potential was fixed at  $E_{\text{ap}} = -1.0 \text{ V}$  ( $10^{-4} \text{ M}$  in viologen units, 12 mL,  $l = 1 \text{ mm}$ ,  $t = \sim 1 \text{ h}$ ).

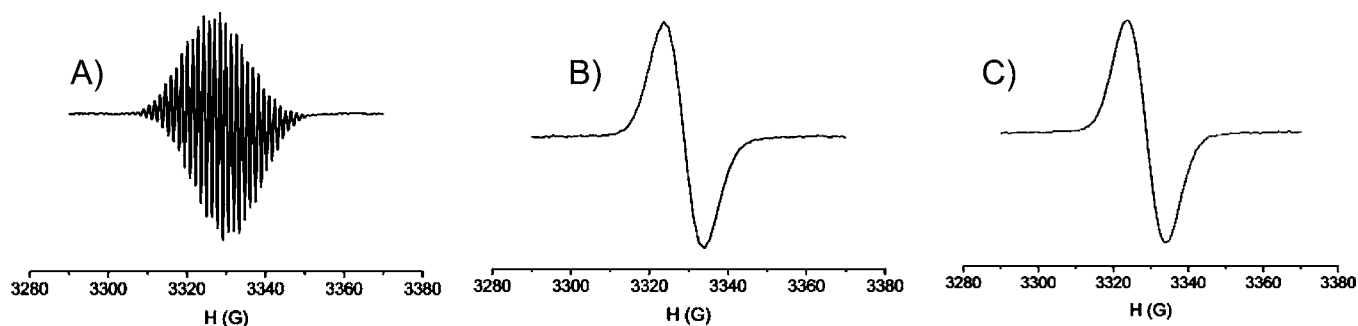


Figure 7. X-band ESR spectra (A)  $\text{DMV}^{2+}$ , (B)  $6^{2(+)}$ , and (C)  $12^{2(+)}$ , recorded at room temperature,  $10^{-4} \text{ M}$  in viologen subunits in DMF + TBAP (0.1 M) (power = 4 mW,  $\nu = 9.355 \text{ Hz}$ , ModAmpl = 0.1 mT).

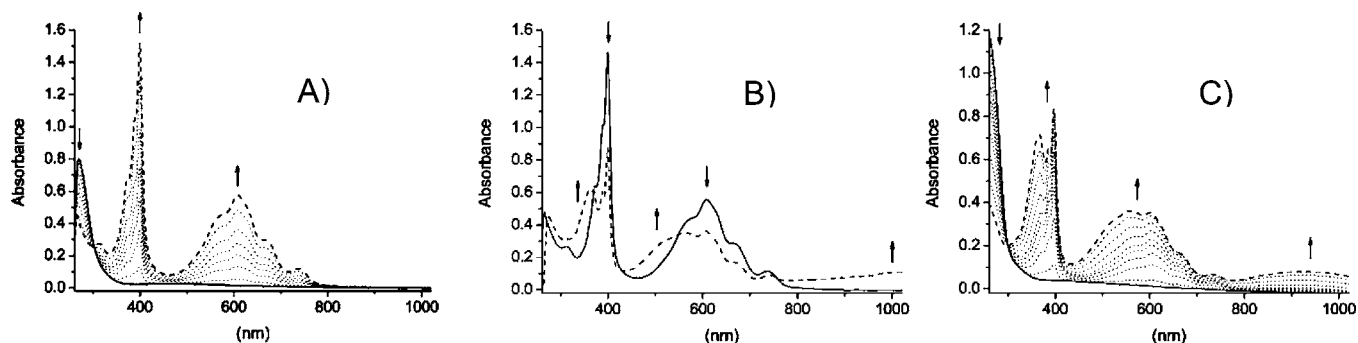
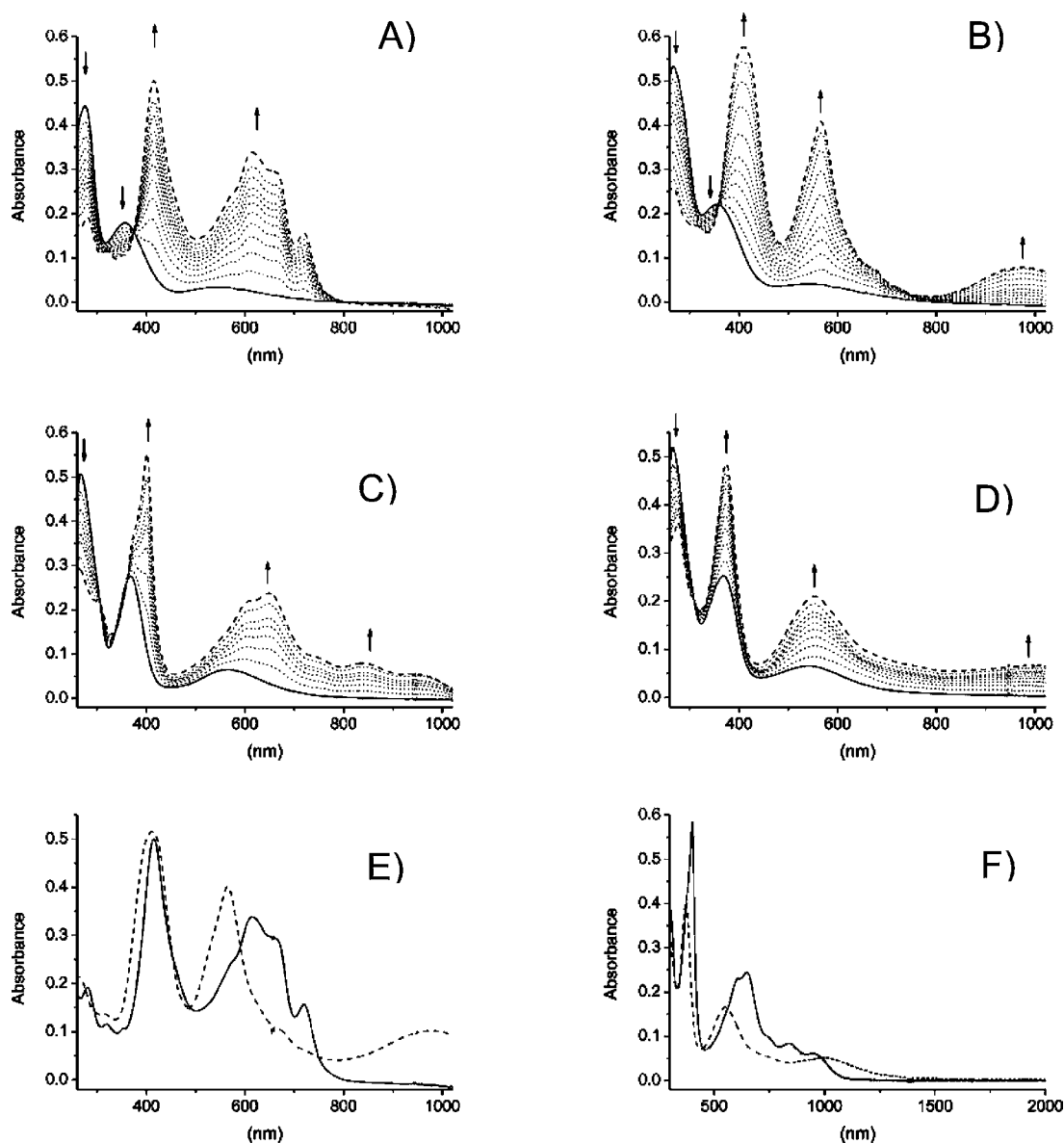


Figure 8. (A) UV-vis spectra recorded during the one-electron reduction (per viologen) of  $12(\text{PF}_6)_4$  (20 mL at  $\sim 4 \times 10^{-5} \text{ M}$  in viologen) conducted at 298 K in DMF/THF 50/50 (v/v) + TBAP (0.1 M) using a platinum working electrode ( $\sim 10 \text{ cm}^2$ ,  $E_{\text{ap}} = -0.9 \text{ V}$ ,  $t \sim 1.4 \text{ h}$ ) and a 10 mm all quartz immersion probe. (B) UV-vis spectra of  $12^{2(+)}$  recorded in DMF/THF 50/50 (v/v) + TBAP (0.1 M) at 298 K (solid line) and after cooling at 193 K (dotted line). (C) UV-vis spectra recorded during the one-electron reduction (per viologen) of  $12(\text{PF}_6)_4$  ( $6 \times 10^{-5} \text{ M}$  in viologen) conducted at 298 K in  $\text{H}_2\text{O}/\text{DMF}$  90/10 (v/v) +  $\text{KNO}_3$  (0.1 M) using a carbon working electrode ( $E_{\text{ap}} = -1 \text{ V}$ ,  $t \sim 30 \text{ min}$ ) and a 10 mm immersion probe.

in water, their exhaustive electrochemical reduction could be successfully achieved in a water/DMF mixture (90/10: v/v) using  $\text{KNO}_3$  as a supporting electrolyte and a carbon foam as working electrode. Every attempt to increase the water ratio systematically led to passivation phenomena resulting from the physisorption of the electrogenerated cation radicals, which are far less polar than the starting materials. Here again, only experiments carried out with the ethylene bridged derivative  $12^{4+}$  yielded spectroscopic signatures suggesting the formation of a novel species, *i.e.* showing absorption bands at different wavelengths than those expected for a simple bipyridinium radical. As shown in Figure 8C, the spectrum recorded after

reduction of  $12^{4+}$  carried out in a water/DMF electrolyte is almost identical to that obtained at low temperature (Figure 8B), with an overall blue shift of the signals corresponding to the bis-radical species  $12^{2(+)}$  and a new broad absorption band above 800 nm. The spectroscopic signatures observed at low temperature or in aqueous media are thus in accordance with the formation of the dimerized species  $[\text{12}]_{\text{Dim}}^{2+}$  from the bis-radical  $12^{2(+)}$ , but the magnitude of the observed modifications also reveals that the associated equilibrium ( $K_{\text{Dim}}$ , Figure 5) is not fully displaced under these conditions and that the self-associated species  $[\text{12}]_{\text{Dim}}^{2+}$  and the nonassociated form  $12^{2(+)}$  coexist in solution. It also needs to be mentioned that the



**Figure 9.** UV-vis spectra recorded during the exhaustive one-electron reduction (per viologen) of (A)  $16(\text{PF}_6)_2$  ( $E_{\text{ap}} = -0.90$  V), (B)  $21(\text{PF}_6)_4$  ( $E_{\text{ap}} = -0.88$  V), (C)  $29(\text{PF}_6)_2$  ( $E_{\text{ap}} = -0.95$  V), or (D)  $32(\text{PF}_6)_4$  ( $E_{\text{ap}} = -0.95$  V) or (E) superimposition of  $16^{+\bullet}$  (solid line) and  $[21]_{\text{Ddim}}^{2+\bullet}$  (dashed line) and (F) superimposition of  $29^{+\bullet}$  (solid line) and  $[32]_{\text{Ddim}}^{2+\bullet}$  (dashed line). All these experiments have been conducted at room temperature on  $\sim 10$  mL of a given receptor ( $10^{-4}$  M in viologen subunits) dissolved in DMF + TBAP (0.1 M), using a platinum plate working electrode ( $\sim 10$  cm<sup>2</sup>, duration of the experiments  $\sim 1$  h) and a 1 mm all quartz immersion probe.

intramolecular nature of this association process is supported by the fact that no modifications of the UV-vis absorption spectrum could be observed under the same experimental conditions with the reference compound  $\text{DMV}^{+\bullet}$ , neither at low temperature nor in an aqueous electrolyte.

Similar investigations were carried out with the phenyl- and ethynyl-linked ferrocene-viologens  $16^{2+}$ ,  $21^{4+}$ ,  $29^{2+}$ , and  $32^{4+}$ , expecting that rigid and less bulky linkers would allow an efficient intramolecular dimerization of the bipyridinium radicals, a process required to stabilize the *syn* conformation of the targeted electrochemically driven pivot. The exhaustive one electron reduction of the reference phenyl-linked mono viologen-ferrocene  $16(\text{PF}_6)_2$  led to drastic changes in its absorption spectra; the most remarkable ones are reminiscent of those observed when producing the cation radical  $\text{DMV}^{+\bullet}$  (Figure 6), being the growth of intense absorption bands in the

visible range at 415 nm ( $\epsilon = 26500$  L $\cdot\text{mol}^{-1}\cdot\text{cm}^{-1}$ ) and between 570 and 720 nm ( $\epsilon = 18000$  L $\cdot\text{mol}^{-1}\cdot\text{cm}^{-1}$ ) (Figure 9A). These changes are thus easily attributed to the simple and clean transformation of  $16^{2+}$  into  $16^{+\bullet}$ , proceeding *via* a well-defined isosbestic point at 380 nm (Figure 9A).

The same experiment carried out with the disubstituted analogue  $21(\text{PF}_6)_4$  yielded a fully different spectrum (Figure 9B) showing bands gradually developing at  $\lambda_{\text{max}} = 410$  nm ( $\epsilon = 54000$  L $\cdot\text{mol}^{-1}\cdot\text{cm}^{-1}$ ) and 570 nm ( $\epsilon = 38000$  L $\cdot\text{mol}^{-1}\cdot\text{cm}^{-1}$ ), blue-shifted as compared to those observed through the reduction of  $16(\text{PF}_6)_2$  (both final spectra are represented in Figure 9E). Most importantly, the reduction of  $21^{4+}$  also yielded a broad diagnostic band for the presence of  $\pi$ -dimer centered at 980 nm ( $\epsilon = 7400$  L $\cdot\text{mol}^{-1}\cdot\text{cm}^{-1}$ ), whose energy is directly related to the electronic-coupling between both bipyridinium radicals.<sup>26,75,111</sup> This spectroscopic imprint is

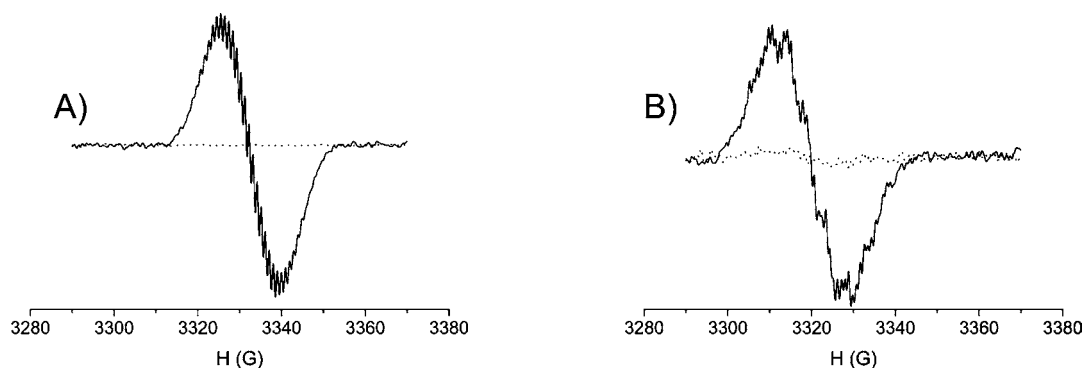


**Figure 10.** X-band ESR spectra of (A)  $16^{+\bullet}$  (solid line) and  $[21^{2+}]_{\text{dim}}$  (dotted line); (B)  $29^{+\bullet}$  (solid line) and  $[32^{2+}]_{\text{dim}}$  (dotted line) recorded at room temperature,  $10^{-4}$  M in viologen subunits dissolved in DMF + TBAP (0.1 M) (power = 4 mW, frequency = 9.355 Hz, ModAmpl = 0.1 mT).

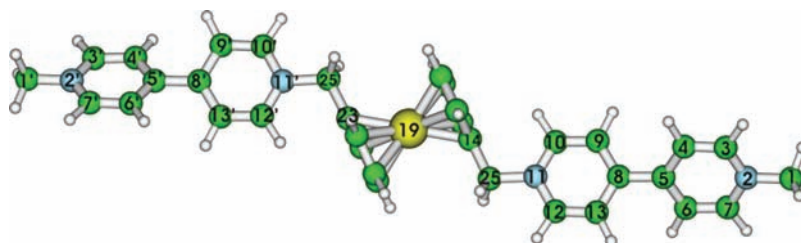


**Figure 11.** Side view of  $6^{4+}$  optimized at the CAM-BLYP/6-31G\* level.

thus a clear evidence of the electron-triggered dimerization leading to  $[21]_{\text{Dim}}^{2+}$ , with the efficiency of this process being demonstrated (i) by the absence of signals attributed to the nonassociated bis-radical species  $21^{2(+\bullet)}$  in the spectrum of the fully electrolyzed solution and (ii) by the observation of one well-defined isosbestic point at 355 nm, suggesting a clean and well-behaved transformation (Figure 9B). This behavior led us to postulate a fast and quantitative electrochemically triggered transformation of the starting tetra-cationic species  $21^{4+}$  into the  $\pi$ -dimer  $[21]_{\text{Dim}}^{2+}$  without experimental evidence suggesting the existence of the intermediate bis-radical  $21^{2(+\bullet)}$ .

The electrochemical reduction of the bipyridinium subunits in the ethynyl-bridged architectures leads to a different set of signals (Figure 9C and D). The electrolysis of the reference compound  $29^{2+}$  into  $29^{+\bullet}$  gives rise to an intense and thin signal at 400 nm ( $\epsilon = 27000 \text{ L}\cdot\text{mol}^{-1}\cdot\text{cm}^{-1}$ ) growing along with a larger one centered at 650 nm ( $\epsilon = 11500 \text{ L}\cdot\text{mol}^{-1}\cdot\text{cm}^{-1}$ ) as well as two bands of weak intensity at 840 nm ( $\epsilon = 3800 \text{ L}\cdot\text{mol}^{-1}\cdot\text{cm}^{-1}$ ) and 950 nm ( $\epsilon = 2600 \text{ L}\cdot\text{mol}^{-1}\cdot\text{cm}^{-1}$ ). The observation of signals over 800 nm in the spectrum of  $29^{+\bullet}$  is quite unexpected, since only the  $\pi$ -dimer-diagnostic bands have so far been observed in the near IR region.<sup>36,38–40,44</sup> This bathochromic shift, in fact, results from the lowering of the  $\pi$ - $\pi^*$  HOMO–LUMO band gap due to the large electronic delocalization occurring between the alkyne-linked donor and acceptor subunits in  $29^{+\bullet}$ .<sup>112</sup>

The spectroscopic signature recorded under the same experimental conditions with the 1,1'-bis(ethynylviologene)-ferrocene  $32^{4+}$  shows two main absorption bands at 375 nm ( $\epsilon = 45500 \text{ L}\cdot\text{mol}^{-1}\cdot\text{cm}^{-1}$ ) and 550 nm ( $\epsilon = 19700 \text{ L}\cdot\text{mol}^{-1}\cdot\text{cm}^{-1}$ ) (Figure 9D), blue-shifted as compared to the signals of the reference radical  $29^{+\bullet}$ , as well as a broad signal centered at 1050 nm. Here again, this spectroscopic response is attributed to a fast and unequivocal formation of the  $\pi$ -dimer  $[32^{2+}]_{\text{dim}}$  from the tetra-cationic derivative  $32^{4+}$ . The superimposition shown in Figure 9F further reveals that the transitions at  $\lambda_{\text{max}} = 375$

and 550 nm in  $[32^{2+}]_{\text{dim}}$  are blue-shifted as compared to those found with the nonassociated radical  $29^{+\bullet}$  and that the broad diagnostic band for the  $\pi$ -dimer appears conversely red-shifted as compared to the signal of lower energy found in the spectrum of  $29^{+\bullet}$ . It needs to be mentioned that the simple and well-defined transformations of  $29^{2+}$  into  $29^{+\bullet}$  as well as that of  $32^{4+}$  into  $[32^{2+}]_{\text{dim}}$  are further demonstrated by the observation of isosbestic points at 305, 340, 360, and 310 nm in the stacked spectra shown in Figure 9C and D, respectively.

The presence of paramagnetic species in each electrolyzed medium has been checked by ESR. The spectra were recorded at room temperature from samples collected after electrochemical reduction (1 electron per viologen) of  $16^{2+}$ ,  $21^{4+}$ ,  $29^{2+}$ , and  $32^{4+}$ . As seen in Figure 10, the mono bipyridium-ferrocenes  $16^{+\bullet}$  and  $29^{+\bullet}$  feature one intense signal at  $g = 2.00$  whereas both 1,1'-disubstituted derivatives were found to be ESR silent, in agreement with the electrochemical and spectroelectrochemical data discussed above, suggesting the formation of the diamagnetic  $\pi$ -dimers  $[21^{2+}]_{\text{dim}}$  and  $[32^{2+}]_{\text{dim}}$ .

**Computational Chemistry.** The present study aims at determining, from a computational point of view, whether the redox properties of the viologens subunits in  $6^{4+}$ ,  $12^{4+}$ ,  $21^{4+}$ , and  $32^{4+}$  can be exploited to promote the rotation of a ferrocene scaffold from an “open” charge-repelled form to a “closed” conformation, wherein the  $\pi$ -orbitals of two bipyridinium cation-radicals would overlap in a face-to-face arrangement (Scheme 1).

Geometry optimization of the nonreduced species  $6^{4+}$ ,  $12^{4+}$ ,  $21^{4+}$ , and  $32^{4+}$  conducted in the gas phase at the CAM-B3LYP<sup>113</sup> level with the 6-31\* basis set (see the Experimental Section and Supporting Information for more detailed information on the calculation procedures) led invariably to open structures wherein both cyclopentadienes adopt a staggered conformation with both dicationic pyridinium substituents pointing toward opposite directions, as seen on the optimized structure of  $6^{4+}$  depicted in Figure 11.  $6^{4+}$ ,  $12^{4+}$ ,

$21^{4+}$ , and  $32^{4+}$  were all found in open conformations, but their exact structure can only be accurately described using the dihedral angle  $\alpha$  defined by the four carbon atoms involved in the ferrocene substitution. For  $6^{4+}$  ( $C_{25}-C_{14}-C_{23}-C_{25}$ , in Figure 11) and for  $32^{4+}$ , this angle was estimated at around  $180^\circ$  (anti conformation) while much lower values were found for  $12^{4+}$  ( $165^\circ$ ) or  $21^{4+}$  ( $169^\circ$ ) (Table 4).

**Table 4.**  $\alpha$ -Angle Values in Gas-Phase DMF (in deg) Calculated<sup>a</sup> for the Nonreduced Species ( $X^{4+}$ ), the Reduced/Nondimerized Species ( $[X]_{\text{open}}^{2(+)}$ ), and the Reduced/Dimerized Species ( $[X]_{\text{dim}}^{2+}$ )<sup>b</sup>

	$\alpha(X^{4+})$	$\alpha([X]_{\text{open}}^{2(+)})$	$\alpha([X]_{\text{dim}}^{2+})$
21	169° (144°)	144° (146°)	8° (2°)
32	180° (142°)	143°	0°
12	165° (141°)	147°	0°
6	179° (177°)	179°	30°

<sup>a</sup>CAM-B3LYP<sup>113</sup>/6-31G\*. <sup>b</sup>Values close to  $180^\circ$  or  $0^\circ$  correspond to staggered conformations whereas values close to  $144^\circ$  correspond to eclipsed conformations.

Calculations were then conducted upon considering DMF as solvent in order to provide theoretical support to experimental data collected in this medium. Under these conditions, optimization of each nonreduced species afforded open conformations with  $\alpha$ -angle values found significantly lower than those measured in the gas phase (Table 4). For instance, angles measured on the minimized conformations of  $21^{4+}$  considered in the gas phase and in solution were estimated at  $169$  and  $144^\circ$ , respectively, with the difference being attributed to the shielding effect of DMF, which decreases the charge repulsion between both solvated dicationic bipyridinium substituents. As opposed to the staggered conformation found in the gas-phase, the angle calculated in DMF ( $\alpha = 144^\circ$ ) corresponds to a situation wherein both iron-linked cyclopentadienes adopt a fully eclipsed arrangement. It should be recalled that the latter is known to be the most stable form of ferrocene (Scheme 5,  $R_1 = R_2 = H$ ), although the associated stabilization energy has been found by electron diffraction studies to be only  $\sim 1$  kcal/mol.<sup>114</sup> This energy gap has been confirmed in the present study with calculations conducted on ferrocene at the CAM-B3LYP level yielding a stabilization for the eclipsed conformation of  $0.55$  and  $0.57$  kcal/mol in the gas phase and DMF solvent, respectively.

The relative energies corresponding to a number of selected conformations adopted by  $21^{4+}$  in DMF were determined by a relaxed scan calculation procedure involving setting the dihedral angle between both bipyridinium substituents ( $\alpha$  in Scheme 5). The energy calculated for  $\alpha = 0^\circ$  ( $E_0$ ) was used as a reference to plot the potential energy surface  $\Delta E = E - E_0$  as a function of the dihedral angle  $\alpha$ . As seen in Figure 12, a minimum is observed when  $\alpha = 144^\circ$  and the energy difference found between this potential well and the less favorable conformation ( $\alpha = 0^\circ$ ) was found to reach  $3.34$  kcal/mol. Fitting these values using the force field Fourier function truncated at the leading term  $F(x) = A(1 + \cos(Bx + C))$  (dashed line in Figure 12) allowed us to estimate  $A = -1.67481$ ,  $B = 1.27674$ , and  $C = 3.14155$ . As seen with the unsubstituted ferrocene, the minimum found on the potential energy surface corresponds to an eclipsed conformation of both cyclopentadienes.

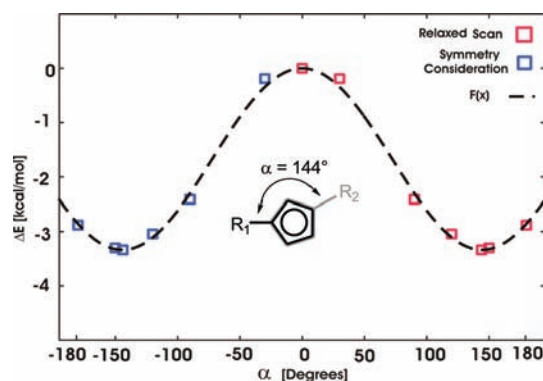


**Figure 12.** Potential energy curve calculated for  $21^{4+}$  in DMF. The red squares are the relaxed scan optimization calculated from  $0^\circ$  to  $180^\circ$ . The blue squares have been obtained considering the C2 symmetry of the complex.  $F(x)$  represents the functional form of the potential with  $F(x) = A(1 + \cos(Bx + C))$  used for fitting.

Detailed theoretical analyses were then carried out on the singlet spin state of the doubly reduced species considered either in open conformations, denoted  $[X]_{\text{open}}^{2(+)}$  ( $\alpha$  values found for each "open" species are collected in Table 4), or as  $\pi$ -dimerized conformers, denoted  $[X]_{\text{dim}}^{2+}$  ( $\alpha = 0^\circ$ ).<sup>115,116</sup>  $\alpha$ -Angles measured on the minimized conformations  $[X]_{\text{open}}^{2(+)}$  were found to range between  $144^\circ$  and  $147^\circ$ , except for the methylene-linked derivative  $[6]_{\text{open}}^{2(+)}$ , exhibiting a much larger  $\alpha$  value of  $179^\circ$  (Table 4). Compound  $[6]_{\text{open}}^{2(+)}$ , furthermore, exhibits two cyclopentadiene rings (Cp) in a staggered conformation, as opposed to  $[12]_{\text{open}}^{2(+)}$ ,  $[21]_{\text{open}}^{2(+)}$ , and  $[32]_{\text{open}}^{2(+)}$ , featuring eclipsed Cp's in their minimized states ( $147 \geq \alpha \geq 143^\circ$ ). The antiparallel orientation ( $\alpha = 179^\circ$ ) of both bipyridinium substituents in  $[6]_{\text{open}}^{2(+)}$  may to some extent be seen as a consequence of a larger charge repulsion effect resulting from the short length of the methylene linker. In the minimized structures, the bisbipyridium cations are furthermore found perpendicular to the Cp rings in  $[12]_{\text{open}}^{2(+)}$  and  $[6]_{\text{open}}^{2(+)}$  whereas they appear almost parallel to the Cp rings in  $[21]_{\text{open}}^{2(+)}$  and  $[32]_{\text{open}}^{2(+)}$ .

The large differences seen in Table 5 between the  $\Delta E$  values calculated for the reduced species in the gas phase and in solution reveal that the closed dimeric conformations  $[X]_{\text{dim}}^{2+}$  are strongly favored by solvent effects, with the largest stabilization being observed for the singlet state  $\pi$ -dimer  $[21]_{\text{dim}}^{2(+)}$ . While looking for parameters that could explain these theoretical results, we found that the large stabilization of the dimeric forms in DMF can be attributed to polarity issues. Dipolar moments computed in DMF solution, ranging from 16 to 37 D for  $[X]_{\text{dim}}^{2+}$  and only from 1 to 9 D for  $[X]_{\text{open}}^{2(+)}$ , indeed reveal that the largest solvent effects ( $\Delta E_{\text{DMF}} - \Delta E_{\text{GP}}$ ) are observed with the most polar species, probably as the results of strong dipole–dipole and ion–dipole interactions occurring with polar DMF molecules (the dipolar moments calculated for  $[21]_{\text{open}}^{2(+)}$  and  $[21]_{\text{dim}}^{2+}$  are represented in Figure 13). In the gas phase,  $[32]_{\text{dim}}^{2+}$ ,  $[21]_{\text{dim}}^{2+}$ , and  $[6]_{\text{dim}}^{2+}$  are found to be the most stable forms by only  $-8.06$ ,  $-2.26$ , and  $-2.15$  kcal/mol, respectively, while, in DMF, their stabilization energies range from  $-17$  to  $-28$  kcal/mol (Table 5). The open conformation  $[X]_{\text{open}}^{2(+)}$  is only found as the most stable form for the ethyl linked ferrocene-viologen ( $X = 12$ ) in the gas phase ( $\Delta E = +1.55$  kcal/mol), but here again, inclusion of DMF allows stabilization of the dimer  $[12]_{\text{dim}}^{2+}$ . In DMF, the lowest  $\Delta E$  values have been obtained with the alkyl-linked derivatives  $6^{2+}$  and  $12^{2+}$ , as the result of steric repulsion issues prohibiting both

**Table 5. Energy Differences Calculated<sup>a</sup> between the Open ( $[X]_{\text{open}}^{2(+*)}$ ,  $\alpha = 144\text{--}179^\circ$ ,  $S = 0$ ) and  $\pi$ -Dimerized ( $[X]_{\text{dim}}^{2+}$ ,  $\alpha = 0^\circ$ ,  $S = 0$ ) Forms of the Doubly Reduced Species  $6^{2(+*)}$ ,  $12^{2(+*)}$ ,  $21^{2(+*)}$ , and  $32^{2(+*)}$  in the Gas Phase ( $\Delta E_{\text{GP}}$ ) and in DMF Solution ( $\Delta E_{\text{DMF}}$ )<sup>b</sup>**

X	$\Delta E_{\text{GP}} = E_{\text{dim}} - E_{\text{open}}$ (kcal/mol)	$\Delta E_{\text{DMF}} = E_{\text{dim,open}}$ (kcal/mol)	$\Delta E_{\text{GP}} - \Delta E_{\text{DMF}}$ (kcal/mol)	total dipolar moment in gas phase (Debye)		total dipolar moment in DMF (Debye)	
				$[X]_{\text{dim}}^{2+}$ $\alpha = 0^\circ$	$[X]_{\text{open}}^{2(+*)c}$ $\alpha = 144^\circ$ $\alpha = 143^\circ$ $\alpha = 147^\circ$ $\alpha = 179^\circ$	$[X]_{\text{dim}}^{2+}$ $\alpha = 0^\circ$	$[X]_{\text{open}}^{2(+*)c}$
21	-2.26	-27.81	25.55	28.4	8.2 (20.2)	36.9	9.3 (27.6)
32	-8.04	-27.74	19.70	15.8	5.6 (10.2)	21.7	6.4 (15.3)
12	+1.55	-21.11	22.66	22.8	3.0 (19.8)	26.7	2.7 (24)
6	-2.15	-18.47	16.32	16.1	0.2 (15.9)	19.3	1.1 (18.2)

<sup>a</sup>CAM-B3LYP<sup>113</sup>/6-31G\*. <sup>b</sup>The closed conformation is favored when  $\Delta E = E_{\text{dim}(0^\circ)} - E_{\text{open}(\alpha)} < 0$ . <sup>c</sup>For each entry, the difference between the dipolar moments calculated for the open ( $[X]_{\text{open}}^{2(+*)}$ ) and closed ( $[X]_{\text{dim}}^{2+}$ ) conformations is shown between parentheses.

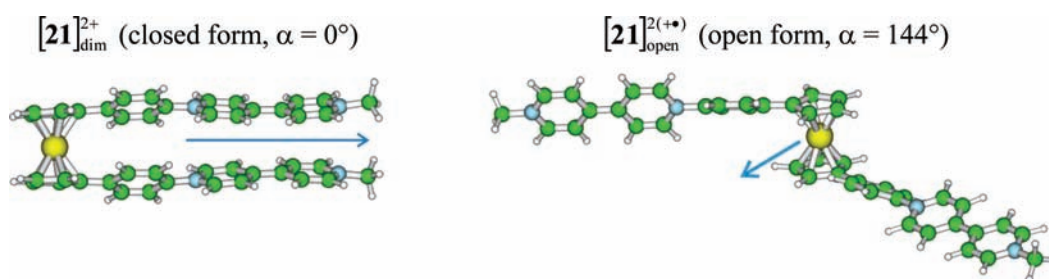


**Figure 13.** Dipolar moments calculated for  $[21]_{\text{open}}^{2(+*)}$  ( $\alpha = 144^\circ$ ) and  $[21]_{\text{dim}}^{2+}$ .

reduced bipyridium substituents from adopting a cofacial arrangement. These steric effects are clearly revealed on the minimized structures of  $[6]_{\text{dim}}^{2+}$  and  $[12]_{\text{dim}}^{2+}$ , for instance through the deformation of the ferrocene scaffold with an angle between both Cp planes reaching  $12.3^\circ$  in  $[6]_{\text{dim}}^{2+}$  whereas much lower values, below  $6^\circ$ , are measured for  $[32]_{\text{dim}}^{2+}$  and  $[21]_{\text{dim}}^{2+}$  (Table 5). The optimized form of  $[6]_{\text{dim}}^{2+}$  (see Figure 26 of the Supporting Information), moreover, reveals that the steric hindrances between both methylene linkers ( $C_{25}\text{--H}$  and  $C_{25}\text{--H}$ ) and between the adjacent ferrocene and pyridinium rings prohibit the formation of a fully symmetric “face to face” arrangement of both bipyridinium cation radicals and, hence, prevent a good overlap of their HOMO orbitals.

Similar constraints due to the bulkiness of the alkyl chains are observed on the minimized structure of  $[12]_{\text{dim}}^{2+}$ , and all our theoretical investigations support the experimental findings suggesting that alkyl linkers are not suited to promote the intramolecular  $\pi$ -dimerizations of both bipyridium cation radicals. The distance between both Cp rings appears indeed too short to avoid the repulsion between the alkyl chains located on the upper and lower Cp rings.

The theoretical predictions obtained for  $21^{4+}$  and  $32^{4+}$  using the CAM-B3LYP<sup>113</sup>/6-31G\* functional are in good agreement with what is observed experimentally. The stabilization energies found for the flexible systems  $6^{4+}$  and  $12^{4+}$  are conversely quite different from what might be expected from the experimental observations. Similar overestimated values have also been obtained for the closed conformations using other DFT functionals (see ESI), namely B3LYP and M06-2X. These discrepancies between experiment and theory are not well understood; however, a common feature of the data obtained with B3LYP, CAM-B3LYP, and M06-2X is that inclusion of

solvent leads to an important stabilization of the closed conformation, with the largest  $\Delta E$  values systematically found for  $21^{4+}$  and  $32^{4+}$ . Solvent effects seem overestimated, but the trend in the series is reliable. The phenyl and alkyne linkers are not only found best suited for the formation of a cofacial arrangement in the  $\pi$ -dimer complex  $[X]_{\text{dim}}^{2+}$ ; they also allow a more straightforward rotation from the charge repelled state to the  $\pi$ -dimer state, with an overall reorganization which is less energetically demanding than the same processes considered with the flexible systems  $6^{4+}$  or  $12^{4+}$ . Structural data found for  $21^{4+}$  and  $32^{4+}$  and for  $[32]_{\text{dim}}^{2+}$  and  $[21]_{\text{dim}}^{2+}$  indeed reveal that the conversions between the open and closed conformation require a large rotation of the ferrocene pivot but involve only little changes for the bipyridium substituents (The effects of electron doping on the angles and bond distances measured on the viologen units are tabulated in Table ESI 2). The result of our molecular orbital analyses carried out with  $[21]_{\text{dim}}^{2+}$  is shown in Figure 14. The LUMO of the open species  $21^{4+}$  becomes the HOMO of the doubly reduced species  $[21]_{\text{dim}}^{2+}$  with a bonding character associated with the C8–C5 (C8'–C5') bonds. The same feature is observed for the C4–C3 (C6–C7) and C9–C10 (C12–C13) bonds, which are also found shorter in the reduced form, as opposed to C4–C5 (C5–C6), N2–C3 (N2–C7), and N10–C11 (N11–C12), whose antibonding character is revealed by their elongated bond lengths (see Table 2 of the Supporting Information). The pictures shown in Figure 14 further reveal that the effective orbital overlaps in the HOMO of  $[21]_{\text{dim}}^{2+}$  are responsible for the efficient association between both radicals yielding the closed  $\pi$ -dimer  $[21]_{\text{dim}}^{2+}$ . In the latter species, the significant electronic delocalization observed over a large  $\pi$  system involving the pyridinium units, the phenyl linker,

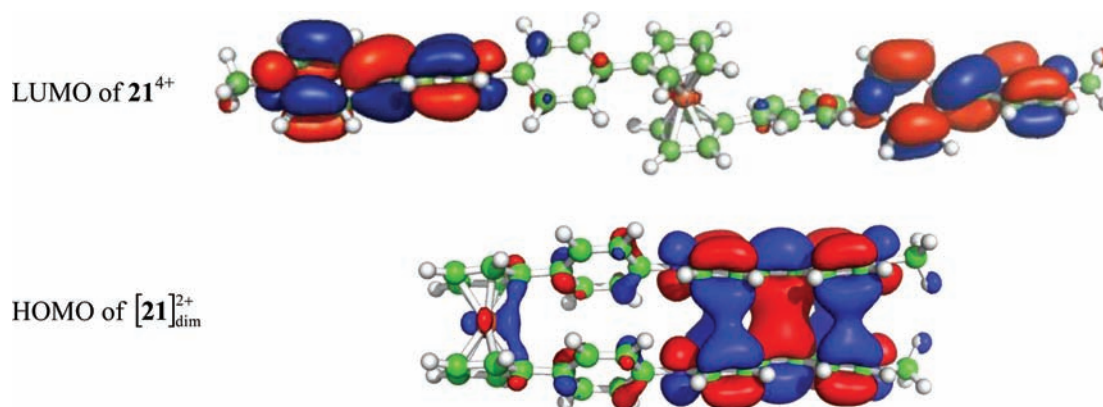


**Figure 14.** Frontier molecular orbitals calculated for (top)  $21^{4+}$  and (bottom)  $[21]_{\text{dim}}^{2+}$ . The electron density isosurface is 0.02 au.

and the ferrocene leads to a stabilization of the closed conformation overstepping the electrostatic repulsion.

## CONCLUSION

We have described the first example of a ferrocene-based redox-responsive molecular carousel whose rotating motion is triggered by simple electron transfers centered on  $\pi$ -dimerizable bipyridinium fragments introduced on both Cp's. Detailed electrochemical, theoretical, and spectroscopic analyses reveal that formation of intramolecular  $\pi$ -dimers requires the introduction of rigid, conjugated organic linkers between the rotating metallocene module and between the electron motive  $\pi$ -dimerizable drivers. Evidence for intramolecular dimerization came from electrochemistry data, supporting the existence of chemical steps coupled to the electron transfer processes, and from ESR and UV-vis spectroscopy with the observation of diagnostic absorption bands, notably in the near-infrared region. All our conclusions were supported by computational investigations which provided key insights into the structure of the self-assembled intramolecular  $\pi$ -dimers and into the conformation of the tetra-cationic "charge-repelled" conformers.

## EXPERIMENTAL SECTION

**General Methods.**  $^1\text{H}$  NMR and  $^{13}\text{C}$  NMR spectra were recorded on Bruker 300 or 400 MHz spectrometers.  $^1\text{H}$  chemical shifts (ppm) were referenced to residual solvent peaks. UV-vis spectra were recorded on an MCS 500 UV-NIR Zeiss spectrophotometer using conventional quartz cells or all-quartz immersion probes (Hellma Inc.). Elemental analyses (C, H, and N) were carried out on a Perkin-Elmer 240 analyzer. ESI or DCI positive mode spectra were recorded with an Esquire 3000 Plus, Bruker Daltonics.

All chemicals were used as received unless otherwise noted. 4,4-Dipyridyl (98%) and 2-bromopyridine (99%) were purchased from Acros and Aldrich, respectively. Anhydrous acetonitrile and DMF were purchased from Rathburn Inc. and Acros, respectively.

Cyclic voltammetry (CV) and voltamperometry at rotating disk electrodes (RDE) were recorded using a CH-600 potentiostat (CH-instrument). All analytical experiments were conducted under an argon atmosphere (glovebox or argon stream) in a standard one-compartment, three-electrode electrochemical cell. Tetra-*n*-butylammonium perchlorate (TBAP) or potassium nitrate ( $\text{KNO}_3$ ) was used as supporting electrolyte (0.1 M) in nonaqueous (DMF) or aqueous media (DMF/ $\text{H}_2\text{O}$ ). An ohmic drop compensation was performed when using cyclic voltammetry. CH-instrument vitreous carbon ( $\varnothing = 3$  mm) or platinum ( $\varnothing = 2$  mm) working electrodes were polished with 1  $\mu\text{m}$  diamond paste before each recording. A standard sweep rate of 0.01  $\text{V}\cdot\text{s}^{-1}$  was used in RDE experiments. Voltamperometry at rotating disk electrode (RDE) was carried out with radiometer

equipment at a rotation rate of 550  $\text{rd}\cdot\text{min}^{-1}$  using a glassy carbon RDE tip ( $\varnothing = 3$  mm).

Spectroelectrochemical measurements were carried out in a glovebox with a standard potentiostat coupled to an MCS 500 UV-NIR Zeiss spectrophotometer using 1 mm or 10 mm all quartz immersion probes. Electrolyses were conducted at 25  $^\circ\text{C}$  using a platinum plate working electrode and a large piece of carbon felt as a counterelectrode isolated from the electrolytic solution through an ionic bridge. A CH instrument  $\text{AgAgNO}_3$  ( $10^{-2}$  M + TBAP  $10^{-1}$  M in  $\text{CH}_3\text{CN}$ ) was used as a reference electrode.

ESR X-band spectra were recorded on a Bruker EMX, equipped with the ER-4192 ST Bruker cavity.

Calculations were performed using the Gaussian09 suite of programs.<sup>117</sup> We used the hybrid exchange-correlation functional CAM-B3LYP<sup>113</sup> based on a B3LYP<sup>118,119</sup> upgraded with the long-range corrections proposed by Tawada et al.<sup>120</sup> For all calculations, we used the well-known basis set 6-31G\* for the C,N,H atoms and the SDD<sup>121</sup> pseudopotential combined with SDD<sup>122</sup> basis sets for the Fe atom. Each structure was optimized in the gas phase and/or in *N,N*-dimethylformamide solution (DMF,  $\epsilon = 37.219$ ) using the polarizable continuum model (PCM).<sup>123–126</sup>

**Syntheses.** The ferrocene-1,1'-dicarboxaldehyde **2** was synthesized according to a procedure described by Pélineski.<sup>127</sup> The synthesis of  $6(\text{PF}_6)_4$  was carried out according to a published procedure developed by Olivier Reynes in our laboratory.<sup>51</sup> The 1-ferrocenyl-4-nitrobenzene **13** and 1-ferrocenylaniline **14** were synthesized following procedures described by D'Souza and Ito.<sup>68</sup> The syntheses of 1,1'-ferrocenyl-bisboronic acid **17** and 1,1'-ferrocenyl-bis(4-bromophenyl) **18** were performed according to a procedure described by Knapp and Rehahn.<sup>73</sup> 2-Bromo-4-iodopyridine **23**,<sup>77</sup> 1-iodoferrocene **27**,<sup>128</sup> and 1,1'-diiodoferrocene **30**<sup>80,82,129</sup> were synthesized following literature procedures.

**Synthesis of 10.** The dialcohol **9** (0.1 g, 0.4 mmol) and dry triethylamine (4 mmol) were dissolved in anhydrous methylene chloride (10 mL). This solution was then purged for 15 min with argon gas and cooled down to  $-5$   $^\circ\text{C}$  using an iced bath of sodium chloride solution. A solution of methanesulfonyl chloride (MsCl) (0.32 mL, 4 mmol) in dry  $\text{CH}_2\text{Cl}_2$  (2 mL) was then added dropwise for 20 min. The resulting mixture was stirred at  $-5$   $^\circ\text{C}$  for 2 h and then overnight at room temperature and subsequently washed with water ( $3 \times 5$  mL) and brine (5 mL). The organic phase was dried over anhydrous  $\text{Na}_2\text{SO}_4$ , filtered, and evaporated under reduced pressure. After the crude product was dissolved in  $\text{CH}_2\text{Cl}_2$  (10 mL), LiBr (1.55 g, 17.8 mmol) was added under argon, and the solution was stirred in the dark at room temperature for 48 h. The reaction mixture was then washed with water, dried over anhydrous  $\text{Na}_2\text{SO}_4$ , and evaporated under reduced pressure. The crude product was purified by column chromatography on  $\text{SiO}_2$  ( $\text{CH}_2\text{Cl}_2/\text{cyclohexane} = 1/1$  v/v) to afford **10** as a yellow powder. Yield: 47% (75 mg).  $^1\text{H}$  NMR (400 MHz,  $\text{CD}_3\text{CN}$ )  $\delta$ : 4.11 (t,  $^3J = 1.8$  Hz, 4H), 4.07 (t,  $^3J = 1.8$  Hz, 4H), 3.49 (t,  $^3J = 7.4$  Hz, 4H), 2.88 (t,  $^3J = 7.4$  Hz, 4H).  $^{13}\text{C}$  NMR (400 MHz,

CD<sub>3</sub>CN)  $\delta$ : 85.57, 68.75, 68.00, 33.00, 32.67. MS (ESI<sup>+</sup>):  $m/z$  399.8 ([M]<sup>+</sup>, 100%). Anal. Calc % for C<sub>14</sub>H<sub>16</sub>Br<sub>2</sub>Fe: C, 42.04; H, 4.03. Found %: C, 42.02; H, 4.49.

**Synthesis of 11(PF<sub>6</sub>)<sub>2</sub>.** To a solution of 4,4'-bipyridine (0.9 mg, 5.8 mmol) in dry acetonitrile (3 mL) was added dropwise the dibromide derivative **10** (0.33 g, 0.08 mmol) in dry acetonitrile (2 mL). The reaction mixture was protected from light and stirred at reflux under argon atmosphere for 2 days. The pink precipitate was filtered and washed with acetonitrile. The solid compound was dissolved in a minimum of water, and the PF<sub>6</sub><sup>-</sup> salt was precipitated by addition of an aqueous saturated solution of KPF<sub>6</sub>. The pink-red solid was filtered and washed with water. Yield: 87% (56.6 mg). <sup>1</sup>H NMR (400 MHz, CD<sub>3</sub>CN)  $\delta$ : 8.84 (d, <sup>3</sup>J = 6.1 Hz, 4H), 8.53 (d, <sup>3</sup>J = 6.9 Hz, 4H), 8.23 (d, <sup>3</sup>J = 6.9 Hz, 4H), 7.76 (d, <sup>3</sup>J = 6.1 Hz, 4H), 4.59 (t, <sup>3</sup>J = 7.0 Hz, 4H), 4.09 (t, <sup>3</sup>J = 1.8 Hz, 4H), 3.96 (t, <sup>3</sup>J = 1.8 Hz, 4H), 3.01 (t, <sup>3</sup>J = 7.0 Hz, 4H). <sup>13</sup>C NMR (300 MHz, CD<sub>3</sub>CN)  $\delta$ : 151.13, 144.71, 125.49, 121.58, 69.02, 62.19, 30.52. MS (ESI<sup>+</sup>):  $m/z$  679 ([M - PF<sub>6</sub>]<sup>+</sup>, 20%), 276 ([M - 2PF<sub>6</sub>]<sup>2+</sup>, 100%). Anal. Calc % for C<sub>34</sub>H<sub>32</sub>F<sub>12</sub>FeN<sub>4</sub>P<sub>2</sub>: C, 48.48; H, 3.83; N, 6.65. Found %: C, 48.54; H, 3.79; N, 6.79.

**Synthesis of 12(PF<sub>6</sub>)<sub>4</sub>.** To a degassed solution of **11**(PF<sub>6</sub>)<sub>2</sub> (58 mg, 0.07 mmol) in acetonitrile (10 mL) was added dropwise CH<sub>3</sub>I (1 g, 0.5 mL, 7 mmol). This solution was then stirred under an argon atmosphere in the dark at 40 °C for 2 days. After cooling, the brown precipitate was filtered, washed thoroughly with acetonitrile, and dissolved into a minimum of water. The addition of an aqueous saturated KPF<sub>6</sub> solution (~1 mL) led to the precipitation of a light pink solid which was filtered, washed with water, and dried. Yield: 50% (40 mg). <sup>1</sup>H NMR (300 MHz, CD<sub>3</sub>CN)  $\delta$  (ppm): 8.84 (d, <sup>3</sup>J = 6.4 Hz, 4H), 8.67 (d, <sup>3</sup>J = 6.4 Hz, 4H), 8.32 (m, 8H), 4.67 (t, <sup>3</sup>J = 6.9 Hz, 4H), 4.40 (s, 6H, CH<sub>3</sub>), 4.11 (s, 4H), 3.99 (s, 4H), 3.05 (t, <sup>3</sup>J = 6.9 Hz, 4H). MS (ESI<sup>+</sup>):  $m/z$  1016.9 ([M - PF<sub>6</sub>]<sup>+</sup>, 5%), 436 ([M - 2PF<sub>6</sub>]<sup>2+</sup>, 20%). Anal. Calc % for C<sub>36</sub>H<sub>38</sub>F<sub>24</sub>FeN<sub>4</sub>P<sub>4</sub>: C, 37.20; H, 3.30; N, 4.82. Found %: C, 36.27; H, 3.04; N, 4.64.

**Synthesis of 15(NO<sub>3</sub>).** 1-Ferrocenyl-4-aniline **14** (0.1 g, 0.372 mmol) and N-(2,4-dinitrophenyl)-4,4'-bipyridinium chloride (0.1 g, 0.248 mmol) were dissolved in a dry mixture of CH<sub>3</sub>CN/EtOH = 1/3 (v/v) (20 mL). The resulting solution was then refluxed under stirring for 16 h. After cooling, the solvents were removed under reduced pressure and the crude product was purified by column chromatography on SiO<sub>2</sub> (THF/H<sub>2</sub>O/KNO<sub>3</sub> = 100/20/4) to afford N-(4-phenyl-N-(4,4'-pyridinium))ferrocene nitrate salt as dark red powder. Yield: 90% (0.107 g). <sup>1</sup>H NMR (400 MHz, CD<sub>3</sub>CN)  $\delta$ : 9.03 (d, <sup>3</sup>J = 7.0 Hz, 2H), 8.89 (dd, <sup>3</sup>J = 4.5 Hz, <sup>4</sup>J = 1.7 Hz, 2H), 8.48 (d, <sup>3</sup>J = 7.0 Hz, 2H), 7.88 (dd, <sup>3</sup>J = 4.5 Hz, <sup>4</sup>J = 1.7 Hz, 2H), 7.84 (d, <sup>3</sup>J = 8 Hz, 2H), 7.65 (d, <sup>3</sup>J = 8 Hz, 2H), 4.87 (t, <sup>3</sup>J = 4 Hz, 2H), 4.49 (t, <sup>3</sup>J = 4 Hz, 2H), 4.09 (s, 5H). <sup>13</sup>C NMR (101 MHz, CD<sub>3</sub>CN)  $\delta$ : 152.29, 145.48, 128.45, 126.99, 125.24, 122.90, 118.30, 71.24, 70.86, 68.13. MS (ESI<sup>+</sup>):  $m/z$  417 ([M - PF<sub>6</sub>]<sup>+</sup>, 100%). Anal. Calc % for C<sub>26</sub>H<sub>21</sub>F<sub>6</sub>FeN<sub>2</sub>P: C, 55.54; H, 3.76; N, 4.98. Found %: C, 51.97; H, 3.71; N, 4.77.

**Synthesis of 16(PF<sub>6</sub>)<sub>2</sub>.** To a degassed solution of **15**(NO<sub>3</sub>) (0.05 g, 0.104 mmol) in a mixture of acetonitrile (10 mL) and CH<sub>2</sub>Cl<sub>2</sub> (2 mL) was added dropwise 0.65 mL of CH<sub>3</sub>I (1.48 g, 10.4 mmol). The resulting solution was stirred under an argon atmosphere in the dark at 70 °C for 24 h. After cooling, the precipitate formed was filtered and washed with acetonitrile. This solid was then dissolved into a minimum of water, and an aqueous saturated solution of KPF<sub>6</sub> (~1 mL) was added until observing a dark pink precipitate. This solid was isolated by filtration, washed with water, and dried. Yield: 60% (45 mg). <sup>1</sup>H NMR (400 MHz, CD<sub>3</sub>CN)  $\delta$ : 9.17 (d, <sup>3</sup>J = 7.1 Hz, 2H), 8.88 (d, <sup>3</sup>J = 6.7 Hz, 2H), 8.55 (d, <sup>3</sup>J = 7.0 Hz, 2H), 8.45 (d, <sup>3</sup>J = 6.6 Hz, 2H), 7.87 (d, <sup>3</sup>J = 8.8 Hz, 2H), 7.68 (d, <sup>3</sup>J = 8.8 Hz, 2H), 4.90–4.87 (m, 2H), 4.52–4.49 (m, 2H), 4.42 (s, 3H, CH<sub>3</sub>), 4.09 (s, 4H). MS (ESI<sup>+</sup>):  $m/z$  577 ([M - PF<sub>6</sub>]<sup>+</sup>, 20%), 216 ([M - 2PF<sub>6</sub>]<sup>2+</sup>, 100%).

**Synthesis of 19.** Into a sealed tube were added 1,1'-ferrocenyl-bis(4-bromophenyl) **18** (160 mg, 0.32 mmol), Cu<sub>2</sub>O (5 mg, 0.032 mmol, 10% mol), and DMF/28% NH<sub>3</sub> in water = 50/50 (v/v) (32 mL). After sealing the tube, this suspension was stirred and heated at 80 °C for 2 days. After cooling down to room temperature, water was added (50 mL). The resulting mixture was extracted with Et<sub>2</sub>O (3 × 50 mL).

The combined organic layers were dried over anhydrous Na<sub>2</sub>SO<sub>4</sub>, filtered, and evaporated to dryness. The crude product was purified by column chromatography on SiO<sub>2</sub> (CHCl<sub>3</sub>/MeOH = 98/2 v/v) and dried to afford **19** as a goldish powder. Yield: 46% (54 mg). <sup>1</sup>H NMR (400 MHz, CD<sub>3</sub>Cl<sub>2</sub>)  $\delta$ : 7.12 (d, <sup>3</sup>J = 8.4 Hz, 4H), 6.55 (d, <sup>3</sup>J = 8.4 Hz, 4H), 4.32 (t, <sup>3</sup>J = 4 Hz, 4H), 4.09 (t, <sup>3</sup>J = 4 Hz, 4H), 3.66 (br s, 4H, NH<sub>2</sub>). <sup>13</sup>C NMR (101 MHz, CD<sub>2</sub>Cl<sub>2</sub>)  $\delta$ : 145.38, 128.28, 127.36, 115.25, 87.48, 70.09, 67.35. MS (ESI<sup>+</sup>):  $m/z$  369 ([M + 1]<sup>+</sup>, 100%), 185 ([M + 2]<sup>2+</sup>, 60%). Anal. Calc % for C<sub>22</sub>H<sub>20</sub>FeN<sub>2</sub>: C, 71.75; H, 5.47; N, 7.61. Found %: C, 69.41; H, 5.38; N, 7.31.

**Synthesis of 20(PF<sub>6</sub>)<sub>2</sub>.** The 1,1'-ferrocenyl-bis-4-aniline **19** (0.095 g, 0.26 mmol) and the N-(2,4-dinitrophenyl)-4,4'-bipyridinium chloride (0.555 g, 1.55 mmol) were dissolved in a mixture of CH<sub>3</sub>CN/EtOH = 1/5 (v/v) (50 mL), and the resulting solution was stirred and heated at 80 °C for 2 days. After cooling to room temperature, the solvents were evaporated to dryness under reduced pressure and the crude product was purified by column chromatography on SiO<sub>2</sub> (THF/H<sub>2</sub>O/KPF<sub>6</sub> = 100/20/4 v/v) and dried to afford **20**(PF<sub>6</sub>)<sub>2</sub> as a dark red powder. Yield: 41% (0.1 g). <sup>1</sup>H NMR (400 MHz, CD<sub>3</sub>CN)  $\delta$ : 8.97 (d, <sup>3</sup>J = 6.9 Hz, 4H), 8.86 (d, <sup>3</sup>J = 8 Hz, 4H), 8.43 (d, <sup>3</sup>J = 6.9 Hz, 4H), 7.82 (d, <sup>3</sup>J = 8 Hz, 4H), 7.66 (d, <sup>3</sup>J = 8.7 Hz, 4H), 7.57 (d, <sup>3</sup>J = 8.7 Hz, 4H), 4.80 (t, <sup>3</sup>J = 4 Hz, 4H), 4.42 (t, <sup>3</sup>J = 4 Hz, 4H). <sup>13</sup>C NMR (101 MHz, CD<sub>3</sub>CN)  $\delta$ : 155.60, 152.29, 145.31, 143.68, 141.71, 128.54, 127.00, 125.05, 122.82, 118.31, 84.18, 73.24, 69.52. MS (ESI<sup>+</sup>):  $m/z$  793 ([M - PF<sub>6</sub>]<sup>+</sup>, 60%), 324 ([M - 2PF<sub>6</sub>]<sup>2+</sup>, 100%). Anal. Calc % for C<sub>42</sub>H<sub>32</sub>F<sub>12</sub>FeN<sub>4</sub>P<sub>2</sub>: C, 53.75; H, 3.44; N, 5.97. Found %: C, 52.71; H, 3.44; N, 6.02.

**Synthesis of 21(PF<sub>6</sub>)<sub>4</sub>.** To a degassed solution of **20**(PF<sub>6</sub>)<sub>2</sub> (0.05 g, 0.053 mmol) in dry acetonitrile (2 mL) was added dropwise 1 mL of CH<sub>3</sub>I (2.3 g, 16 mmol). The resulting solution was stirred under an argon atmosphere in the dark at 80 °C for 16 h. After cooling, the precipitate formed was filtered and thoroughly washed with acetonitrile. This solid was then dissolved into a mixture of CH<sub>3</sub>CN/H<sub>2</sub>O/KPF<sub>6</sub> = 100/10/2 (v/v) until complete dissolution. This solution was concentrated under reduced pressure until a dark pink solid was observed. This product was isolated by filtration, washed with water, and dried. Yield: 78% (52 mg). <sup>1</sup>H NMR (400 MHz, CD<sub>3</sub>CN)  $\delta$ : 9.20 (d, <sup>3</sup>J = 6.8 Hz, 4H), 8.90 (d, <sup>3</sup>J = 6.6 Hz, 4H), 8.59 (d, <sup>3</sup>J = 6.8 Hz, 4H), 8.48 (d, <sup>3</sup>J = 6.5 Hz, 4H), 7.77 (d, <sup>3</sup>J = 8.7 Hz, 4H), 7.70 (d, <sup>3</sup>J = 8.7 Hz, 4H), 4.83 (s, 4H), 4.43 (s, 6H, CH<sub>3</sub>), 4.37 (s, 4H). MS (ESI<sup>+</sup>):  $m/z$  1113 ([M - PF<sub>6</sub>]<sup>+</sup>, 40%), 484.0 ([M - 2PF<sub>6</sub>]<sup>2+</sup>, 100%). Anal. Calc % for C<sub>44</sub>H<sub>38</sub>F<sub>24</sub>FeN<sub>4</sub>P<sub>4</sub>: C, 41.99; H, 3.04; N, 4.45. Found %: C, 40.72; H, 3.01; N, 4.61.

**Synthesis of 24.** A solution of 2-bromo-4-iodopyridine **23** (2.3 g, 8.1 mmol) and pyridine-4-boronic acid (1 g, 8.1 mmol), and NaHCO<sub>3</sub> (2.72 g, 32.4 mmol) dissolved in a mixture of 1,2-dimethoxyethane (DME) and water (150 mL of DME/H<sub>2</sub>O = 70:30 v/v), was degassed through a freeze-pump-thaw procedure (3 cycles). Tetrakis-(triphenylphosphine)palladium(0) (0.5 g, 0.43 mmol, 20% mol) was then added, and the stirred mixture was heated at 120 °C under an argon atmosphere for 16 h. After cooling to room temperature, the solvents were removed under reduced pressure and the solid product was dissolved in dichloromethane (100 mL) and then washed with 0.1 M aqueous NaOH (100 mL) and with water (3 × 100 mL). The organic layer was dried over anhydrous Na<sub>2</sub>SO<sub>4</sub>, filtered, and evaporated to dryness under reduced pressure to give a brown solid. The crude product was purified by column chromatography on SiO<sub>2</sub> (CH<sub>2</sub>Cl<sub>2</sub>/CH<sub>3</sub>OH/Et<sub>3</sub>N = 473/25/2) to afford **24** as a white powder. Yield: 64% (0.64 g). <sup>1</sup>H NMR (400 MHz, DMSO-*d*<sub>6</sub>)  $\delta$ : 8.73 (dd, <sup>3</sup>J = 4.5 Hz, <sup>4</sup>J = 1.6 Hz, 2H), 8.54 (d, <sup>3</sup>J = 5.2 Hz, 1H), 8.12 (d, <sup>3</sup>J = 1.2 Hz, 1H), 7.90 (dd, <sup>3</sup>J = 5.2 Hz, <sup>4</sup>J = 1.6 Hz, 1H), 7.86 (dd, <sup>3</sup>J = 4.5 Hz, <sup>4</sup>J = 1.6 Hz, 2H). <sup>13</sup>C NMR (101 MHz, DMSO-*d*<sub>6</sub>)  $\delta$ : 151.24, 150.58, 147.76, 142.83, 142.54, 125.40, 121.49, 121.14. MS (DCI):  $m/z$  235 ([M]<sup>+</sup>, 100%). Anal. Calc % for C<sub>10</sub>H<sub>7</sub>BrN<sub>2</sub>: C, 51.09; H, 3.00; Br, 33.99; N, 11.92. Found %: C, 51.49; H, 3.15; N, 12.05.

**Synthesis of 25.** 2-Bromo-4,4'-bipyridine **24** (2.14 g, 9.1 mmol) was added into a two-neck round-bottom flask equipped with a condenser/septum-stopcock and an addition funnel containing [PdCl<sub>2</sub>(1,1'-bis(diphenylphosphino)ferrocene)] (0.2 g, 0.36 mmol, 4% mol) and CuI (0.17 g, 0.91 mmol, 10% mol). This setup was purged 3 times



with vacuum/argon cycles before a degassed mixture of triethyl amine in dry THF was added (150 mL of Et<sub>3</sub>N/THF = 1/2 v/v). The Pd- and Cu-based catalysts were then added and the stirred reaction mixture, kept under an argon atmosphere, was heated at 45 °C for 1 day. After cooling to room temperature, the mixture was filtered and the remaining solid was washed with CH<sub>3</sub>Cl (~10 mL). The filtrate was washed with water, dried over anhydrous Na<sub>2</sub>SO<sub>4</sub> and then filtered and evaporated under reduced pressure to give a brown oil. This crude product was purified by column chromatography on SiO<sub>2</sub> using ethyl acetate/Et<sub>3</sub>N = 99/1 (v/v) to afford **25** as a light brown powder. Yield: 96% (2.2 g). <sup>1</sup>H NMR (400 MHz, DMSO-*d*<sub>6</sub>) δ: 8.71 (d, <sup>3</sup>J = 4.8 Hz, 2H), 8.69 (d, <sup>3</sup>J = 5.2 Hz, 1H), 7.98 (s, 1H), 7.88 (d, <sup>3</sup>J = 4.8 Hz, 2H), 8.85 (d, <sup>3</sup>J = 5.2 Hz, 1H), 0.27 (s, 9H, CH<sub>3</sub>). MS (ESI<sup>+</sup>): *m/z* 253 ([M]<sup>+</sup>, 100%).

**Synthesis of 26.** A solution of **25** (2.2 g, 8.7 mmol) in methanol (22 mL) and 1 N aqueous NaOH (9 mL) was stirred for 90 min at room temperature. Acetic acid (9 mL) was then added, and the mixture was brought to dryness under reduced pressure. The solid residue was washed with diethyl ether (~20 mL), and the filtrate was washed with water (3 × 20 mL) and then with brine (1 × 20 mL), dried over anhydrous Na<sub>2</sub>SO<sub>4</sub>, filtered, and finally evaporated under reduced pressure. The crude product was purified by column chromatography on SiO<sub>2</sub> (CH<sub>2</sub>Cl<sub>2</sub>/CH<sub>3</sub>OH/Et<sub>3</sub>N = 96/3/1). Yield: 66% (1.04 g). <sup>1</sup>H NMR (400 MHz, DMSO-*d*<sub>6</sub>) δ: 8.74 (d, <sup>3</sup>J = 6.4 Hz, 2H), 8.69 (d, <sup>3</sup>J = 6.4 Hz, 1H), 8.01 (d, <sup>3</sup>J = 1.7 Hz, 1H), 7.89–7.85 (m, 3H), 4.43 (s, 1H, ethynyl). <sup>13</sup>C NMR (101 MHz, DMSO-*d*<sub>6</sub>) δ: 152.01, 151.58, 146.10, 146.04, 144.42, 143.71, 125.74, 122.37, 122.34, 83.99, 81.79, 55.91. MS (DCI): *m/z* 181 ([M + 1]<sup>+</sup>, 100%), 209 ([M + C<sub>2</sub>H<sub>5</sub>]<sup>+</sup>, 30%).

**Synthesis of 28.** 1-Iodoferrocene **27** (0.064 g, 0.355 mmol) and the 2-ethynyl-4,4'-bipyridine **26** (0.111 g, 0.355 mmol) were added into a two-neck round-bottom flask equipped with a stopcock-fitted condenser and an addition funnel containing dichloro((bis-(diphenylphosphino)ferrocenyl)palladium(II) (0.03 g, 0.04 mmol, 10% mol) and CuI (0.01 g, 0.04 mmol, 10% mol). This setup was purged 3 times with vacuum/argon cycles before a degassed mixture of triethyl amine in dry THF (Et<sub>3</sub>N/THF = 1/2 v/v) (9 mL) was added over the stirred mixture of 1-iodoferrocene and 2-ethynyl-4,4'-bipyridine. The Cu- and Pd-based catalysts were added, and the reaction mixture was stirred and heated at 80 °C for 24 h. After cooling to room temperature, the solid phase was filtered and washed with CH<sub>3</sub>Cl (~10 mL). The filtrate was washed with water (3 × 25 mL) and dried over anhydrous Na<sub>2</sub>SO<sub>4</sub>. After filtration, the solvents were removed under reduced pressure, and the crude product was purified by column chromatography on SiO<sub>2</sub> (CHCl<sub>3</sub>/CH<sub>3</sub>OH = 98/2 v/v) to afford **28** as an orange powder. Yield: 26% (33 mg). <sup>1</sup>H NMR (300 MHz, CD<sub>2</sub>Cl<sub>2</sub>) δ: 8.76 (d, <sup>3</sup>J = 6.2 Hz, 2H), 8.67 (d, <sup>3</sup>J = 5.2 Hz, 1H), 7.73 (d, <sup>3</sup>J = 3 Hz, 1H), 7.63 (d, <sup>3</sup>J = 6.2 Hz, 2H), 7.48 (d, <sup>3</sup>J = 5.2 Hz, 1H), 4.61 (t, <sup>3</sup>J = 3 Hz, 2H), 4.34 (t, <sup>3</sup>J = 3 Hz, 2H), 4.28 (s, 5H). MS (ESI<sup>+</sup>): *m/z* 365 ([M + 1]<sup>+</sup>, 100%).

**Synthesis of 29(PF<sub>6</sub>)<sub>2</sub>.** CH<sub>3</sub>I (1.7 mL, 28 mmol) was added dropwise to a degassed solution of 1-(2-ethynyl-4,4'-bipyridine)-ferrocene **28** (0.029 g, 0.08 mmol) dissolved in a mixture of acetonitrile (2 mL) and dichloromethane (0.5 mL). This solution was stirred under an argon atmosphere in the dark at 40 °C for 24 h. After cooling to room temperature, the dark precipitate was filtered and washed thoroughly with acetonitrile. This intermediate was dissolved into a minimum of water, and the addition of a saturated aqueous KPF<sub>6</sub> solution (~1 mL) resulted in the precipitation of a purple solid. This final product was filtered, washed with water, and dried. Yield: 51% (27.5 mg). <sup>1</sup>H NMR (400 MHz, DMSO-*d*<sub>6</sub>) δ: 9.30–9.27 (m, 3H), 8.91 (d, <sup>3</sup>J = 4 Hz, 1H), 8.79 (d, <sup>3</sup>J = 8 Hz, 2H), 8.61 (dd, <sup>3</sup>J = 8 Hz, <sup>4</sup>J = 4 Hz, 1H), 4.9 (t, <sup>3</sup>J = 2 Hz, 2H), 4.69 (t, <sup>3</sup>J = 2 Hz, 2H), 4.00 (m, 11H). MS (ESI<sup>+</sup>): *m/z* 539 ([M - PF<sub>6</sub>]<sup>+</sup>, 30%), 197 ([M - 2PF<sub>6</sub>]<sup>2+</sup>, 100%).

**Synthesis of 31.** 1,1'-Diiodoferrocene **30** (0.325 g, 0.74 mmol) and 2-ethynyl-4,4'-bipyridine **26** (0.667 g, 3.7 mmol) were introduced into a two-neck round-bottom flask equipped with a stopcock-fitted condenser and an addition funnel containing tetrakis-(triphenylphosphine)palladium(0) (0.171 g, 0.14 mmol, 5% mol)

and CuI (0.14 g, 0.74 mmol, 10% mol). This setup was purged 3 times with vacuum/argon cycles and then a degassed solution of triethyl amine in dry THF (60 mL of Et<sub>3</sub>N/THF = 1/2 v/v) was added over the stirred mixture of 1,1'-diiodoferrocene and 2-ethynyl-4,4'-bipyridine. The Cu- and Pd-based catalysts were then added, and the reaction mixture was heated at 70 °C under stirring for 60 h. After cooling to room temperature, insoluble materials were filtered and washed with CH<sub>3</sub>Cl (~10 mL). The filtrate was washed with water (3 × 10 mL) and dried over anhydrous Na<sub>2</sub>SO<sub>4</sub>. After filtration, the solvents were removed under reduced pressure to afford a crude product containing 2-ethynyl-4,4'-bipyridine, 1-(2-ethynyl-4,4'-bipyridine)-1-iodoferrocene, and 1,1'-bis(2-ethynyl-4,4'-bipyridine)-ferrocene. This mixture was purified by column chromatography on SiO<sub>2</sub> (CH<sub>2</sub>Cl<sub>2</sub>/CH<sub>3</sub>OH = 95/5 v/v) to afford **31** as an orange powder. Yield: 5% (21 mg). <sup>1</sup>H NMR (400 MHz, CD<sub>2</sub>Cl<sub>2</sub>) δ: 8.68 (d, <sup>3</sup>J = 4.8 Hz, 4H), 8.40 (d, <sup>3</sup>J = 5.1 Hz, 2H), 7.55 (s, 2H), 7.43 (d, <sup>3</sup>J = 4.4 Hz, 4H), 7.25 (d, <sup>3</sup>J = 5.1 Hz, 2H), 4.69 (s, 4H), 4.44 (s, 4H). MS (ESI<sup>+</sup>): *m/z* 543 ([M + 1]<sup>+</sup>, 100%), 272 ([M + 2]<sup>2+</sup>, 50%).

**Synthesis of 32(PF<sub>6</sub>)<sub>4</sub>.** CH<sub>3</sub>I was added dropwise (0.7 mL, 11.6 mmol) to a degassed solution of 1,1'-bis(2-ethynyl-4,4'-bipyridine)-ferrocene **31** (0.018 g, 0.033 mmol) in a mixture of acetonitrile (3 mL) and dichloromethane (4 mL). The resulting solution was stirred under an argon atmosphere in the dark at 40 °C for 24 h. After cooling to room temperature, the dark precipitate was filtered and washed with acetonitrile. This solid was dissolved into a minimum of water, and the addition of a saturated aqueous KPF<sub>6</sub> solution (~1 mL) resulted in the precipitation of a purple solid which was filtered, washed with water, and dried. Yield: 60% (23.4 mg). <sup>1</sup>H NMR (400 MHz, D<sub>2</sub>O) δ: 9.08 (d, <sup>3</sup>J = 6.8 Hz, 4H), 9.01 (d, <sup>3</sup>J = 6.7 Hz), 8.64 (d, <sup>3</sup>J = 1.8 Hz, 2H), 8.53 (d, <sup>3</sup>J = 6.8 Hz, 4H), 8.36 (dd, <sup>3</sup>J = 6.6 Hz, <sup>4</sup>J = 2.2 Hz, 2H), 5.10 (t, <sup>3</sup>J = 1.9 Hz, 4H), 4.88 (t, <sup>3</sup>J = 1.9 Hz, 4H), 4.53 and 4.52 (s, 12H, CH<sub>3</sub>). MS (ESI<sup>+</sup>): *m/z* 1037 ([M - PF<sub>6</sub>]<sup>+</sup>, 70%), 446 ([M - 2PF<sub>6</sub>]<sup>2+</sup>, 100%).

## ■ ASSOCIATED CONTENT

### ● Supporting Information

Characterization data and procedure for estimation of *K*<sub>dim</sub>. This material is available free of charge via the Internet at <http://pubs.acs.org>.

## ■ AUTHOR INFORMATION

### Corresponding Author

christophe.bucher@ujf-grenoble.fr

## ■ ACKNOWLEDGMENTS

The authors would like to thank the CNRS, UJF, and “Région Rhône-Alpes”, as well as the “Communauté d'agglomération Grenoble-Alpes Métropole” (Nanobio program) for funding. C.B. and A.I. would also like to express their gratitude to Dr. Damien Jouvenot for sharing his skills in graphic arts.

## ■ REFERENCES

- (1) Kay, E. R.; Leigh, D. A.; Zerbetto, F. *Angew. Chem., Int. Ed.* **2007**, *46*, 72.
- (2) Spruell, J. M.; Coskun, A.; Friedman, D. C.; Forgan, R. S.; Sarjeant, A. A.; Trabolzi, A.; Fahrenbach, A. C.; Barin, G.; Paxton, W. F.; Dey, S. K.; Olson, M. A.; Benítez, D.; Tkatchouk, E.; Colvin, M. T.; Carmielli, R.; Caldwell, S. T.; Rosair, G. M.; Hewage, S. G.; Duclairioir, F.; Seymour, J. L.; Slawin, A. M. Z.; Goddard III, W. A.; Wasielewski, M. R.; Cooke, G.; Stoddart, J. F. *Nat. Chem.* **2010**, *2*, 870.
- (3) Coskun, A.; Spruell, J. M.; Barin, G.; Fahrenbach, A. C.; Forgan, R. S.; Colvin, M. T.; Carmielli, R.; Benítez, D.; Tkatchouk, E.; Friedman, D. C.; Sarjeant, A. A.; Wasielewski, M. R.; Goddard, W. A. III; Stoddart, J. F. *J. Am. Chem. Soc.* **2011**, *133*, 4538.
- (4) Li, H.; Fahrenbach, A. C.; Coskun, A.; Zhu, Z.; Barin, G.; Zhao, Y.-L.; Botros, Y. Y.; Sauvage, J.-P.; Stoddart, J. F. *Angew. Chem., Int. Ed.* **2011**, *50*, 6782.

- (5) Kottas, G. S.; Clarke, L. I.; Horinek, D.; Michl, J. *Chem. Rev.* **2005**, *105*, 1281.
- (6) Hawthorne, M. F.; Ramachandran, B. M.; Kennedy, R. D.; Knobler, C. B. *Pure Appl. Chem.* **2006**, *78*, 1299.
- (7) Vacek, J.; Michl, J. *Adv. Funct. Mater.* **2007**, *17*, 730.
- (8) Vicario, J.; Katsonis, N.; Ramon, B. S.; Bastiaansen, C. M.; Broer, D. J.; Feringa, B. L. *Nature* **2006**, *440*, 163.
- (9) Leigh, D. A.; Wong, J. K. Y.; Dehez, F.; Zerbetto, F. *Nature* **2003**, *424*, 174.
- (10) Kelly, T. R.; De Silva, H.; Silva, R. A. *Nature* **1999**, *401*, 150.
- (11) Koumura, N.; Zijlstra, R. W. J.; Van Delden, R. A.; Harada, N.; Feringa, B. L. *Nature* **1999**, *401*, 152.
- (12) Van Delden, R. A.; Wiel, M. K. J. t.; Pollard, M. M.; Vicario, J.; Koumura, N.; Feringa, B. L. *Nature* **2005**, *437*, 1337.
- (13) Bohn, R. K.; Haaland, A. J. *Organomet. Chem.* **1966**, 470.
- (14) Gardner, A. B.; Howard, J.; Waddington, T. C.; Richardson, R. M.; Tomkinson, J. *Chem. Phys.* **1981**, *57*, 453.
- (15) Brydges, S.; Harrington, L. E.; McGlinchey, M. J. *Coord. Chem. Rev.* **2002**, *233/234*, 75.
- (16) Crowley, J. D.; Steele, I. M.; Bosnich, B. *Chem.—Eur. J.* **2006**, *12*, 8935.
- (17) Wang, X. B.; Dai, B.; Woo, H.-K.; Wang, L.-S. *Angew. Chem., Int. Ed. Engl.* **2005**, *44*, 6022.
- (18) Tanaka, K.; Kinbara, K. *Mol. Biosyst.* **2008**, *4*, 512.
- (19) Zhang, D.; Zhang, Q.; Su, J.; Tian, H. *Chem. Commun.* **2009**, 1700.
- (20) Muraoka, T.; Kinbara, K.; Aida, T. *Nature* **2006**, *440*, 512.
- (21) Muraoka, T.; Kinbara, K.; Aida, T. *J. Am. Chem. Soc.* **2006**, *128*, 11600.
- (22) Muraoka, T.; Kinbara, K.; Kobayashi, Y.; Aida, T. *J. Am. Chem. Soc.* **2003**, *125*, 5612.
- (23) Muraoka, T.; Kinbara, K.; Aida, T. *Chem. Commun.* **2007**, 1441.
- (24) Kinbara, K.; Muraoka, T.; Aida, T. *Org. Biomol. Chem.* **2008**, *6*, 1871.
- (25) Kochi, J. K.; Rathore, R.; Le Magueres, P. *J. Org. Chem.* **2000**, *65*, 6826.
- (26) Lu, J.-M.; Rosokha, S. V.; Kochi, J. K. *J. Am. Chem. Soc.* **2003**, *125*, 12161.
- (27) Nishinaga, T.; Komatsu, K. *Org. Biomol. Chem.* **2005**, *3*, 561.
- (28) Miller, L. L.; Mann, K. R. *Acc. Chem. Res.* **1996**, *29*, 417.
- (29) Levillain, E.; Roncali, J. *J. Am. Chem. Soc.* **1999**, *121*, 8760.
- (30) Hapiot, P.; Audebert, P.; Monnier, K.; Pernaut, J.-M.; Garcia, P. *Chem. Mater.* **1994**, *6*, 1549.
- (31) Fuhrhop, J. H.; Wasser, P.; Riesner, D.; Mauzerall, D. *J. Am. Chem. Soc.* **1972**, *94*, 7796.
- (32) Koivisto, B. D.; Ichimura, A. S.; McDonald, R.; Lemaire, M. T.; Thompson, L. K.; Hick, R. G. *J. Am. Chem. Soc.* **2006**, *128*, 690.
- (33) Femoni, C.; Iapalucci, M. C.; Longoni, G.; Tiozzo, C.; Wolowska, J.; Zacchini, S.; Zazzaroni, E. *Chem.—Eur. J.* **2007**, *13*, 6544.
- (34) Park, J. W.; Choi, N. H.; Kim, J. H. *J. Phys. Chem.* **1996**, *100*, 769.
- (35) Trabolsi, A.; Khashab, N.; Fahrenbach, A. C.; Friedman, D. C.; Colvin, M. T.; Coti, K. K.; Benitez, D.; Tkatchouk, E.; Olsen, J.-C.; Belowich, M. E.; Carmielli, R.; Khatib, H. A.; Goddard, W. A.; Wasielewski, M. R.; Stoddart, J. F. *Nat. Chem.* **2010**, *2*, 42.
- (36) Furue, M.; Nozakura, S.-I. *Chem. Lett.* **1980**, 821.
- (37) Deronzier, A.; Galland, B.; Viera, E. *Nouv. J. Chim.* **1982**, *6*, 97.
- (38) Geuder, W.; Huenig, S.; Suchy, A. *Tetrahedron* **1986**, *42*, 1665.
- (39) Kannappan, R.; Bucher, C.; Saint-Aman, E.; Moutet, J.-C.; Milet, A.; Oltean, M.; Méta, E.; Pellet-Rostaing, S.; Lemaire, M.; Chaix, C. *New J. Chem.* **2010**, *34*, 1373.
- (40) Neta, P.; Richoux, M.-C.; Harriman, A. *J. Chem. Soc., Faraday Trans. 2* **1985**, *81*, 1427.
- (41) Van Leeuwen, J. W.; Van Dijk, C.; Veeger, C. *Eur. J. Biochem.* **1983**, *135*, 601.
- (42) Geuder, W.; Hünig, S.; Suchy, A. *Angew. Chem., Int. Ed. Engl.* **1983**, *22*, 489.
- (43) Itoh, M.; Kosower, E. M. *J. Am. Chem. Soc.* **1968**, *90*, 1843.
- (44) Imabayashi, S.-I.; Kitamura, N.; Tazuke, S.; Tokuda, K. *J. Electroanal. Chem.* **1988**, *243*, 143.
- (45) Coutouli Argyropoulou, E.; Kelaidopoulou, A.; Sideris, C.; Kokkinidis, G. *J. Electroanal. Chem.* **1999**, *477*, 130.
- (46) Fontani, M.; Peters, F.; Scherer, W.; Wachter, W.; Wagner, M.; Zanello, P. *Eur. J. Inorg. Chem.* **1998**, *10*, 1453.
- (47) Kubo, T.; Shinada, T.; Kobayashi, Y.; Imafuku, H.; Toya, T.; Akita, S.; Nishikitani, Y.; Watanabe, H. *Solid State Ionics* **2003**, *165*, 209.
- (48) Meyerhans, A.; Pfau, W.; Memming, R.; Margaretha, P. *Helv. Chim. Acta* **1982**, *65*, 2603.
- (49) Nishikitani, Y.; Ikai, K.; Kobayashi, M.; Imafuku, H.; Minami, M.; Kubo, T. PCT Int. Appl. WO 2000049454 A1 20000824, 2000.
- (50) Fujihira, M.; Yamada, H. *Thin Solid Films* **1988**, *160*, 125.
- (51) Reynes, O.; Bucher, C.; Moutet, J.-C.; Royal, G.; Saint-Aman, E. *Chem. Commun.* **2004**, 428.
- (52) Gonsalves, K.; Zhan-ru, L.; Rausch, M. D. *J. Am. Chem. Soc.* **1984**, *106*, 3862.
- (53) Ratajczak, A.; Czech, B.; Drobek, L. *Syn. React. Inorg. Met.* **1982**, *12*, 557.
- (54) Christensen, T. B.; Ditte, R.; Daasbjerg, K.; Skrydstrup, T. *Chem. Commun.* **1999**, 20, 2051.
- (55) Bhatt, J.; Fung, B. M.; Nicholas, K. M. *Liq. Cryst.* **1992**, *12*, 263.
- (56) Bhattacharyya, S. *J. Org. Chem.* **1998**, *63*, 7101.
- (57) Bhattacharyya, S. *Synlett* **1998**, *8*, 837.
- (58) Hisatome, M.; Takano, S.-I.; Yamakawa, K. *Tetrahedron Lett.* **1985**, *26*, 2347.
- (59) Lopic, J.; Ropic, V. *Croat. Chem. Acta* **2000**, *73*, 755.
- (60) Emmert, B.; Roh, N. *Chem. Ber.* **1925**, *58*, 503.
- (61) Zincke, T. *Liebigs Ann. Chem.* **1904**, *330*, 361.
- (62) Allen, J. G. Brit. Patent GB1399595 (A), 1975.
- (63) Allen, J. G. *Ger. Offen.* DE2527638, 1976.
- (64) Cheng, W.-C.; Kurth, M. J. *Org. Prep. Proced. Int.* **2002**, *34*, 585.
- (65) Anderson, T. *Liebigs Ann. Chem.* **1855**, *94*, 358.
- (66) Weinmayr, V. *J. Am. Chem. Soc.* **1955**, *77*, 3012.
- (67) Carlescu, I.; Scutaru, A. M.; Apreutesei, D.; Alupe, V.; Scutaru, D. *Appl. Organomet. Chem.* **2007**, *21*, 661.
- (68) D'Souza, F.; Smith, P. M.; Gadde, S.; McCarty, A. L.; Kullman, M. J.; Zandler, M. E.; Ito, M.; Araki, Y.; Ito, O. *J. Phys. Chem. B* **2004**, *108*, 11333.
- (69) Beer, P. D.; Sikanyika, H. *Polyhedron* **1990**, *9*, 1091.
- (70) Braga, D.; D'Addario, D.; Polito, M.; Grepioni, F. *Organometallics* **2004**, *23*, 2810.
- (71) Braga, D.; Polito, M.; Braccacini, M.; D'addario, D.; Tagliavini, E.; Proserpio, D. M.; Grepioni, F. *Chem. Commun.* **2002**, 1080.
- (72) Braga, D.; Polito, M.; Braccacini, M.; D'Addario, D.; Tagliavini, E.; Sturba, L.; Grepioni, F. *Organometallics* **2003**, *22*, 2142.
- (73) Knapp, R.; Rehahn, M. *J. Organomet. Chem.* **1993**, *452*, 235.
- (74) Bunnnett, J. F.; Zahler, R. E. *Chem. Rev.* **1951**, *49*, 273.
- (75) Monk, P. M. S. *The viologens: physicochemical properties, synthesis and applications of the salts of 4,4' bipyridine*; Wiley: 1998.
- (76) Miyaura, N.; Suzuki, A. *Chem. Rev.* **1995**, *95*, 2457.
- (77) Duan, X.-F.; Li, X.-H.; Li, F.-Y.; Huang, C.-H. *Synthesis* **2004**, *16*, 2614.
- (78) Sonogashira, K.; Tohda, Y.; Hagihara, N. *Tetrahedron Lett.* **1975**, *16*, 4467.
- (79) Kagan, H. B.; Diter, P.; Gref, A.; Guillaneux, D.; Masson-Szymczak, A.; Rebiere, F.; Riant, O.; Samuel, O.; Taudien, S. *Pure Appl. Chem.* **1996**, *68*, 29.
- (80) Butler, I. R.; Hobson, L. J.; Macan, S. M. E.; Williams, D. J. *Polyhedron* **1993**, *12*, 1901.
- (81) Clarke, P.; Hounslow, A. M.; Keough, R. A.; Lincoln, S. F.; Wainwright, K. P. *Inorg. Chem.* **1990**, *29*, 1793.
- (82) Rausch, M. D.; Ciappenelli, D. J. *J. Organomet. Chem.* **1967**, *10*, 127.
- (83) Gelin, F.; Thummel, R. P. *J. Org. Chem.* **1992**, *57*, 3780.
- (84) Inouye, M.; Hyodo, Y.; Nakazumi, H. *J. Org. Chem.* **1999**, *64*, 2704.

- (85) Kasahara, A.; Izumi, T.; Yoshida, Y.; Shimizu, I. *Bull. Chem. Soc. Jpn.* **1982**, *55*, 1901.
- (86) Shimizu, I. *Bull. Chem. Soc. Jpn.* **1983**, *56*, 2023.
- (87) Shimizu, I.; Kamei, Y.; Tezuka, T.; Izumi, T.; Kasahara, A. *Bull. Chem. Soc. Jpn.* **1983**, *56*, 192.
- (88) Li, H. L.; Fahrenbach, A. C.; Dey, S.; Basu, S.; Trabolsi, A.; Zhu, Z.; Botros, Y. Y.; Stoddard, J. F. *Angew. Chem., Int. Ed.* **2010**, *49*, 8260.
- (89) Hmadeh, M.; Fahrenbach, A. C.; Basu, S.; Trabolsi, A.; Benitez, D.; Li, H.; Albrecht-Gary, A.-M.; Elhabiri, M.; Stoddard, J. F. *Chem.—Eur. J.* **2011**, *17*, 6076.
- (90) Trabolsi, A.; Fahrenbach, A. C.; Dey, S. K.; Share, A. I.; Friedman, D. C.; Basu, S.; Gasa, T. B.; Khashab, N. M.; Saha, S.; Arahamian, I.; Khatib, H. A.; Flood, A. H.; Stoddard, J. F. *Chem. Commun.* **2010**, *46*, 871.
- (91) Li, H.; Zhao, Y.-L.; Fahrenbach, A. C.; Kim, S.-Y.; Paxton, W. F.; Stoddard, J. F. *Org. Biomol. Chem.* **2011**, *9*, 2240.
- (92) Hunter, C. A.; Lawson, K. R.; Perkins, J.; Urch, C. J. *J. Chem. Soc., Perkin Trans. 2* **2001**, 651.
- (93) Hunter, C. A.; Sanders, J. K. M. *J. Am. Chem. Soc.* **1990**, *112*, 5525.
- (94) Farrugia, L. J. *J. Appl. Crystallogr.* **1997**, *30*, 565.
- (95) Richardson, D. E.; Taube, H. *Inorg. Chem.* **1981**, *20*, 1278.
- (96) Bird, C. L.; Kuhn, A. T. *Chem. Soc. Rev.* **1981**, *10*, 49.
- (97) Deronzier, A. *Electrochim. Acta* **1983**, *28*, 805.
- (98) Ammar, F.; Saveant, J. M. *J. Electroanal. Chem.* **1973**, *47*, 115.
- (99) Bard, A. J. *Pure Appl. Chem.* **1971**, *25*, 379.
- (100) Atherton, S. J.; Tsukahara, K.; Wilkins, R. G. *J. Am. Chem. Soc.* **1986**, *108*, 3380.
- (101) Pedatsur, N.; Richoux, M.-C.; Harriman, A. *J. Chem. Soc., Faraday Trans. 2* **1985**, *81*, 1427.
- (102) Jeon, W. S.; Kim, H.-J.; Lee, C.; Kim, K. *Chem. Commun.* **2002**, 1828.
- (103) Di Matteo, A. *Chem. Phys. Lett.* **2007**, *439*, 190.
- (104) Armstrong, A. T.; Smith, F.; Elder, E.; McGlynn, S. P. *J. Chem. Phys.* **1967**, *46*, 4321.
- (105) Sporer, C.; Ratera, I.; Ruiz-Molina, D.; Vidal-Gancedo, J.; Ventosa, N.; Wurst, K.; Jaitner, P.; Rovira, C.; Veciana, J. *Solid State Sci.* **2009**, *11*, 786.
- (106) Sporer, C.; Ratera, I.; Wurst, K.; Vidal-Gancedo, J.; Ruiz-Molina, D.; Rovira, C.; Veciana, J. *Arkivoc* **2005**, *ix*, 104.
- (107) Alain, V. *Inorg. Chim. Acta* **1996**, *242*, 43.
- (108) Johnson, C. S. G. *J. Chem. Phys.* **1963**, *39*, 58.
- (109) Rieger, A. L.; Rieger, P. H. *J. Phys. Chem.* **1984**, *88*, 5845.
- (110) Water is known to favor the dimerization of viologen cation radicals. This effect most probably results from the hydrophobicity of the reduced forms. See ref 72 for more detailed informations.
- (111) Lee, C.; Lee, Y. M.; Moon, M. S.; Park, S. H.; Park, J. W.; Kim, K. G.; Jeon, S.-J. *J. Electroanal. Chem.* **1996**, *416*, 139.
- (112) Gomila, R. M.; Garau, C.; Frontera, A.; Quiñero, D.; Ballester, P.; Costa, A.; Deyà, P. M. *Tetrahedron Lett.* **2004**, *45*, 9387.
- (113) Yanai, T.; Tew, D.; Handy, N. *Chem. Phys. Lett.* **2004**, *393*, 51.
- (114) Haaland, A. *Acc. Chem. Res.* **1979**, *12*, 415.
- (115) Calculations conducted in the gas phase revealed that both species are minima of the PES (Potential Energy Surface).
- (116) For calculations including solvent effects, we used geometries optimized in the gas phase to stress the influence of the solvent on the stabilization energy of the closed form. It should be noted that experiments conducted with compound **21** revealed that the changes in geometry are small or negligible.
- (117) Frisch, M. J.; Trucks, G. W.; Schlegel, H. B.; Scuseria, G. E.; Robb, M. A.; Cheeseman, J. R.; Scalmani, G.; Barone, V.; Mennucci, B.; Petersson, G. A.; Nakatsuji, H.; Caricato, M.; Li, X.; Hratchian, H. P.; Izmaylov, A. F.; Bloino, J.; Zheng, G.; Sonnenberg, J. L.; Hada, M.; Ehara, M.; Toyota, K.; Fukuda, R.; Hasegawa, J.; Ishida, M.; Nakajima, T.; Honda, Y.; Kitao, O.; Nakai, H.; Vreven, T.; Montgomery, J. A., Jr.; Peralta, J. E.; Ogliaro, F.; Bearpark, M.; Heyd, J. J.; Brothers, E.; Kudin, K. N.; Staroverov, V. N.; Kobayashi, R.; Normand, J.; Raghavachari, K.; Rendell, A.; Burant, J. C.; Iyengar, S. S.; Tomasi, J.; Cossi, M.; Rega, N.; Millam, N. J.; Klene, M.; Knox, J. E.; Cross, J. B.; Bakken, V.; Adamo, C.; Jaramillo, J.; Gomperts, R.; Stratmann, R. E.; Yazyev, O.; Austin, A. J.; Cammi, R.; Pomelli, C.; Ochterski, J. W.; Martin, R. L.; Morokuma, K.; Zakrzewski, V. G.; Voth, G. A.; Salvador, P.; Dannenberg, J. J.; Dapprich, S.; Daniels, A. D.; Farkas, Ö.; Foresman, J. B.; Ortiz, J. V.; Cioslowski, J.; Fox, D. J. *Gaussian 09, Revision C.02*; Gaussian, Inc.: Wallingford, CT, 2009.
- (118) Becke, A. D. *J. Chem. Phys.* **1993**, *98*, 5648.
- (119) Lee, C. T.; Yang, W. T.; Parr, R. G. *Phys. Rev. B* **1988**, *37*, 785.
- (120) Tawada, Y.; Tsuneda, T.; Yanagisawa, S.; Yanai, T.; Hirao, K. *J. Chem. Phys.* **2004**, *120*, 8425.
- (121) Dolg, M.; Wedig, U.; Stoll, H.; Preuss, H. *J. Chem. Phys.* **1987**, *86*, 866.
- (122) Dunning, T. H., Jr.; Hay, P. J. In *Modern Theoretical Chemistry*, Third Edition; Schaefer, H. F., Ed.; Plenum: New York, 1976; Vol. 3, pp 1–28.
- (123) Cancès, M. T.; Mennucci, B.; Tomasi, J. *J. Chem. Phys.* **1997**, *107*, 3032.
- (124) Cossi, M.; Barone, V.; Mennucci, B.; Tomasi, J. *Chem. Phys. Lett.* **1998**, *286*, 253.
- (125) Mennucci, B.; Tomasi, J. *J. Chem. Phys.* **1997**, *106*, 5151.
- (126) Cossi, M.; Scalmani, G.; Rega, N.; Barone, V. *J. Chem. Phys.* **2002**, *117*, 43.
- (127) Bastin, S. *Tetrahedron: Asymmetry* **1999**, *10*, 1647.
- (128) Guillaneux, D.; Kagan, H. B. *J. Org. Chem.* **1995**, *60*, 2502.
- (129) Wright, M. E. *Organometallics* **1990**, *9*, 853.